The cosmic-ray events around AD 775 and AD 993 - Assessing their causes and possible effects on climate

Florian Mekhaldi

Dissertations in Geology at Lund University,
Master's thesis, no 412
(45 hp/ECTS credits)

Department of Geology
Lund University
2014

The cosmic-ray events around AD 775 and AD 993 - Assessing their causes and possible effects on climate

Master's thesis

Florian Mekhaldi

Department of Geology
Lund University
2014

Contents

Abbreviations

AMS	Accelerator mass spectrometry
b2k	Before AD 2000
CCN	Cloud condensation nuclei
CFA	Continuous flow analysis
CWT	Continuous wavelet transform
F_{30}	Fluence (particles per cm^2) above 30 MeV
GCR	Galactic cosmic-rays
GICC05	Greenland Ice Core Chronology 2005
GLE	Ground level event
GRB	Gamma-ray burst
GRIP	Greenland Ice core Project
M12-M13 events	The cosmic-ray events related to the discovery of rapid increases in radiocarbon content measured in Japanese cedar trees by Miyake et al. (2012, 2013)
MeV	Million electronvolt
NAO	North Atlantic oscillation
NGRIP	North Greenland Ice core Project
PCA	Principal component analysis
SCR	Solar cosmic-rays
SEP	Solar energetic particles
SPE	Solar proton event
SPE05	Solar proton event of 20th January 2005
SPE56	Solar proton event of 23rd February 1956
SPE72	Solar proton event of 4th August 1972
$T_{1/2}$	Half-life of radioactive nuclide
$\Delta^{14}C$	^{14}C concentration corrected for fractionation and decay, relative to a standard

The cosmic-ray events around AD 775 and AD 993 - Assessing their causes and possible effects on climate

FLORIAN MEKHALDI

Mekhaldi, F., 2014: The cosmic-ray events around AD 775 and AD 993 - Assessing their causes and possible effects on climate. *Dissertations in Geology at Lund University*, No. 412, 41 pp. 45 hp (45 ECTS credits)

Abstract: Miyake et al. (2012, 2013) discovered rapid increases of ^{14}C content in tree rings dated to AD 774/5 and AD 992/3 which were attributed to unprecedented cosmic-ray events. These extreme particle events have no counterparts in the instrumental and historical record and consequently praised great interest. Indeed, many studies have tentatively associated the two events to solar proton events (SPE), supernovae, gamma-ray bursts (GRB) and to a cometary event which all differ in terms of their energy spectrum. Furthermore, such outbursts of energetic particles have the potential to deplete atmospheric ozone and impact atmospheric circulation and temperature. In consequence, the aims of this project were twofold. The first and most emphasized was to assess the likelihood for the different suggested causes. The second was to investigate the possible effects of the cosmic-ray events on climate.

Cosmogenic radionuclides such as ^{10}Be, ^{14}C and ^{36}Cl arise from the nuclear cascade which is triggered when cosmic-rays reach the atmosphere. These radio-isotopes are produced through different reaction pathways which have different energy dependencies. This discriminant feature could consequently help to better constrain the energy of the incident particles and thus the origin of the two events. Nevertheless, only ^{14}C has been measured so far at annual resolution. In that light, new annually-resolved ^{10}Be was measured from the NGRIP ice core and used in complement with available records of other radionuclides. An exhaustive and very highly-resolved dataset of ions and element compounds from the NGRIP ice core in addition to $\delta^{18}O$ records from several Greenland ice cores were utilized in order to investigate the potential effects on climate.

The results demonstrate that ^{10}Be concentrations and flux from the NGRIP ice core also exhibit large increases in relation to both events and similar to those reported in tree rings ^{14}C content. This symmetric increase in both radionuclides suggests solar proton events as a cause for both cosmic-ray events. Furthermore, the multiple cosmogenic radionuclide records show that both events were measured around the globe in both hemispheres which is also fully consistent with solar proton events. Calculations based on the different production yields of ^{10}Be, ^{14}C and ^{36}Cl indicate that the two probable SPEs were characterized by a hard spectrum and by unprecedented fluences. As a matter of fact, it is found that the solar flare responsible for the larger of the two events (AD 774/5) was an order of magnitude stronger than the hardest instrumental SPE. More startlingly, it was substantially more energetic than the Carrington event of 1859 which is considered as the strongest reported historical solar flare. Coeval peaks in Pb, Cd and Na ice core concentrations suggest an atmospheric circulation response timed with the larger of the two events. The high Na concentrations are interpreted as increased vigor in marine air masses associated with sustained storminess in the North Atlantic synchronous with the exceptional SPE. Finally, the new NGRIP ^{10}Be measurements from this study shed light on the existence of an unexpected early offset in the Greenland Ice Core Chronology 2005 (GICC05) time scale. Lags of 4 years at AD 993 and of 7 years at AD 775 in GICC05 are reported.

Keywords: cosmic-rays, cosmogenic radionuclides, GICC05, NGRIP, solar proton event, storminess

Supervisor: Raimund Muscheler

Co-supervisor: Florian Adolphi

Florian Mekhaldi, Department of Geology, Lund University, Sölvegatan 12, SE-223 62 Lund, Sweden.
E-mail: florian.mekhaldi@gmail.com

Kosmisk strålnings händelsena runt år 775 och år 993 – Utvärdera orsaker och möjliga effekter på klimatet

FLORIAN MEKHALDI

Mekhaldi, F., 2014: Kosmisk strålnings händelsena runt år 775 och år 993 – Utvärdera orsaker och möjliga effekter på klimatet. *Examensarbeten i geologi vid Lunds universitet*, Nr. 412, 41 sid. 45 hp (45 ECTS credits)

Sammanfattning: Miyake et al. (2012,2013) upptäckte en snabb ökning av ^{14}C i träringar daterade till 774/5 och 992/3 vilket tillskrevs exceptionalla kosmik strålnings händelser. Dessa extrema partikel händelser har inget motstycke i instrumentala eller hstoriska arkiv och blev följdaktigen mycket uppmärksammade. Många studier har försöt koppla samman dessa två händelser med sol protonstormar (SPE), supernovor, gamma strålnings utbrott och med att en komet passerat genom atmosfären, alla dessa skiljer sig ifråga om energi spektrum. Vidare har sådana utbrott av hög energi partiklar potential att utarma atmosfäriskt ozon och påverka atmosfärens cirkulation och temperature. Som konsekvens av detta har detta projekt två mål. Det första och mest betonade målet var att bestämma sannolikheten för de olika föreslagna orsakerna. Det andra var att utreda möjliga effekter av kosmik strålnings händelser på klimatet.

Kosmiska radionuklider som ^{10}Be, ^{14}C och ^{36}Cl uppstår från den nuclear cascade som startas av att kosmiska strålar når atmosfären. Dessa radioaktiva isotoper produceras genom olika reaktions vägar som har olika energi behov. Detta diskriminerade särdrag kan följdaktigen användas för att ringa in energin på moderpartiklarna och därigenom ursprunget till de två händelserna. Dock har endast ^{14}C mätts med årlig upplösning än så länge. I ljus av detta gjordes nya ^{10}Be mätningar med en årlig upplösning på NGRIP iskärnan och användes tillsamans med tillgänglig data över andra radionuklider. Ett uttömande och mycket högupplöst dataset för joner och grundämnen från NGRIP iskärnan sammt $\delta^{18}O$ arkiv från flera Iskärnor från Grönland användes för att utreda den potentiella effekten på klimatet.

Resultaten demonstrerar att ^{10}Be concentrationer och flöde i NGRIP iskärnan också uppvisar stora ökningar i relation till båda händelserna liknande de förändringar i ^{14}C som påvisats i träringar. Denna symetriska ökningen i båda radionukliderna indikerar att sol protonstormar var orsaken till båda kosmik strålnings händelserna. Vidare visar ett flertal arkiv över kosmogeniska radionuklider att båda händelserna uppmättes runt hela klotet i båda hemisfärerna också är konsekvent med sol protonstormar. Beräkningar baserade på produktionen av ^{10}Be, ^{14}C och ^{36}Cl indikerar att de två troliga SPE karaktäriserades av ett hårt spektrum och saknade motstycke avseende fluenser. Faktum är att solutbrottet som orsakade den största av de två händelserna (774/5) var en magnitud större än den hårdaste instrumentellt uppmäta SPEn. Mer överaskande hade den avsevärt mycket högre energi än Carrington händelsen 1859 som anses vara den starkaste av de rapporterade historiska sol protonstormar. Sammtidiga toppar i Pb, Cd och Na i iskärnan indikerar en reaktion i den atmosfäriska cirkulationen simultant med den större av de två händelserna. Den höga Na koncentrationen tolkas som ökad styrka i luftmassor associerad med ökad stormighet över norra atlanten sammtidigt med den exceptionella SPE. Slutligen, de nya ^{10}Be mätningarna i NGRIP iskärnan från denna studie påvisar existensen av en oförutsedd *offset* i the Greenland Ice Core Chronology 2005 (GICC05) tidskalan. Förseningar om fyra år vid år 993 och om sju år vid år 775 i GICC05 påvisas.

Nyckelord : GICC05, kosmisk strålning, kosmogeniska radionuklider, NGRIP, protonstorm, stormighet

Handledare: Raimund Muscheler

Bihandledare : Florian Adolphi

Florian Mekhaldi, Geologiska institutionen, Lunds universitet, Sölvegatan 12, SE-223 62 Lund, Sverige.
E-post: florian.mekhaldi@gmail.com

1 Introduction

This project was motivated by the discovery of two unprecedented signatures of rapid increase in $\Delta^{14}C$ measured in Japanese cedar trees (fig. 1) dated to AD 774/5 and AD 992/3 (Miyake et al., 2012; 2013). Cosmogenic radionuclides such as ^{10}Be, ^{14}C and ^{36}Cl arise from the nuclear cascade which is triggered when cosmic-rays penetrate in the atmosphere and interact with nitrogen, oxygen and argon. On annual to centennial time scales, the amount of cosmic-rays reaching the atmosphere is chiefly dictated by the intensity of the heliomagnetic field (Muscheler et al., 2007) which acts as a shield. Hence the concentration of radionuclides, as found in geological archives, is not constant and oscillates through time. However, the larger of the two mentioned rapid increases (AD 774/5) was characterized by a sharp enhancement in ^{14}C content of 12‰ over 1 year which is about 20 times larger than changes attributed to ordinary solar modulation (Miyake et al., 2012). As a result, the AD 774/5 and AD 992/3 increases in radiocarbon (thereafter M12 and M13 events respectively) were linked to exceptional cosmic-ray events which have no counterpart in the instrumental records. It should be mentioned that increases in ^{10}Be from the Antarctic ice core Dome Fuji (Horiuchi et al., 2008) are also discernible during these periods although only measured at a resolution of 10-15 years.

The discovery of the exceptionally energetic M12 and M13 events has led to many studies tentatively attributing them to several astrophysical sources. Initially, Miyake et al. (2012) argued that neither a supernova nor a solar flare could be responsible because the energies required would be too high. Subsequently, Melott & Thomas (2012) and Usoskin et al. (2013) revisited the calculations of the former authors and suggested that an extremely strong solar proton event could in fact represent a possible source for the rapid increases seen in ^{14}C and ^{10}Be. Furthermore, Hambaryan & Neuhauser (2013) as well as Pavlov et al. (2013) claimed that a gamma-ray burst could also potentially explain the cosmic outbursts of energetic particles around AD 775 and AD 993. More recently, Liu et al. (2014) measured the M12 event in coral skeletons and linked it to a coeval cometary event.

Cosmogenic ^{10}Be, ^{14}C and ^{36}Cl are produced in the atmosphere through different reaction pathways. Moreover, their individual production rate cross-sections are differently sensitive to the energies of incident particles. Owing to this, one could theoretically deduce the energy spectrum and therefore the causes of the two events. However, only ^{14}C has been used so far at annual resolution in order to investigate the causes of the M12 and M13 events.

Besides the intriguing nature of these cosmic events and the impact they would have on today's technological society they may also be climatically relevant. Indeed, the fact that such outbursts of energetic particles occurred in the vicinity of Earth also raises the question of how did the atmosphere and the climate system react to them. For instance, it has been suggested that galactic cosmic-rays and solar particles could play an important role in cloud coverage (Svensmark & Friis-Christensen, 1997; Tinsley, 2000; Voiculescu et al., 2006). Alternatively, solar particles are known to cause ozone depletion in the high latitudes of the stratosphere (eg. Jackman et al., 1990; Seppala et al., 2004) which could potentially lead to significant climate cooling (Melott & Thomas, 2012) and/or atmospheric circulation changes in the troposphere.

Better assessing the origin of the M12 and M13 events is consequently of great importance for our understanding of the dynamics of the sun and other stars, for space weather forecasting and for space engineering. It is also very interesting for investigating how cosmic-rays and/or solar particles can impact weather and climate. In consequence, the aims of this study are twofold. First and most importantly, new and annually-resolved ^{10}Be was measured from the ice core North Greenland Ice Core Project (NGRIP) and complemented with other available cosmogenic radionuclides records in order to assess the causes of the M12 and M13 events. Second, the potential impact of the two events on climate was investigated using a very highly-resolved and extensive dataset of ions and

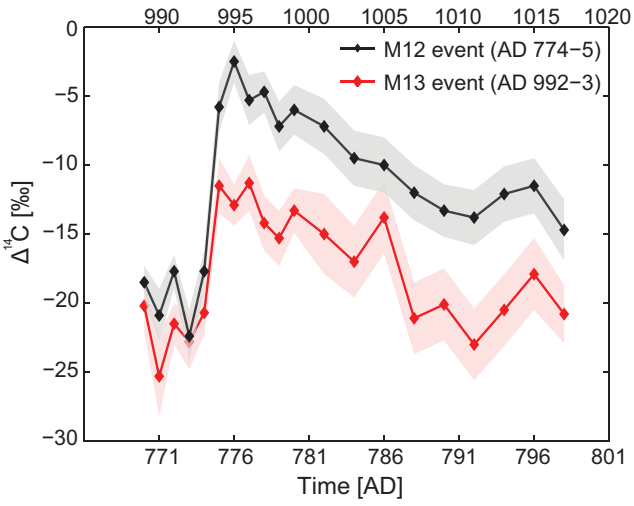

Fig. 1. The rapid increases in $\Delta^{14}C$ seen during the M12 and M13 events. Modified from Miyake et al. (2013).

element compounds measured in NGRIP and provided by McConnell et al. (unpublished). Additional climate proxies from Greenland ice cores were also considered.

2 Background

The scientific background of cosmic radiation and subsequent cosmogenic radionuclides production, transport and deposition and their interaction within the atmosphere is crucial to the understanding of this study. Herein is presented a comprehensive description on cosmic rays and induced radionuclides as well as on the suggested link between energetic particles and atmospheric chemistry and thereby climate.

2.1 Cosmic-rays

Cosmic rays are mainly composed of hydrogen nuclei (protons) and helium nuclei (α-particles) stripped of their orbital electrons - respectively ~87% and ~12% (Beer et al., 2012). The latter particles are accelerated at velocities approaching the speed of light and are continually bombarding Earth´s atmosphere (Friedlander 1989). Our planet is, to some extent, shielded from cosmic radiation by the geomagnetic field and by the heliosphere (solar modulation). Both vary in intensity through time and modulate the amount of energetic particles reaching the atmosphere. As such, periods of strong solar activity would result in fewer particles reaching Earth and conversely (fig. 2 – upper panel).

Cosmic rays have arguably a wide energy spectrum with the softer end (< 1 GeV) namely explained by particles emanating from the Sun (Solar Cosmic Rays-SCR) while particles irradiated from beyond the Heliopause (Galactic Cosmic Rays-GCR) make up the harder end of the spectrum (> 1GeV). GCRs mainly originate from supernovae which occur on average every 30-50 years (Beer et al., 2012). Supernovae represent the violent core-collapse of massive stars triggered by the lack of supply of nuclear fuel (Schawinski et al., 2008). During the explosion, heavy and rare elements are expelled while pulsars, gamma-ray bursts (GRB) and even black holes can be produced. Ejected material and interstellar shocked material constitute supernovae remnants which are bound by shock waves. These are believed to be the source of acceleration of the energetic particles constituting galactic cosmic rays (Koyama et al., 1995).

However in this study, the unprecedented rapid-increases in cosmic radiation yielded a radiocarbon change about 20 times larger than attributed to ordinary solar modulation (Miyake et al., 2012). This suggests that the origin(s) of the M12 and M13 events (AD 774/5 and AD 992/3 respectively) is different. There are several candidates which could potentially explain such a rapid increase: solar proton events (SPE), short GRBs, relatively close SNs or dust from a comet. These different astrophysical sources vary in terms of their energy spectrum.

This diverging feature will be the key of this study for assessing the origin of the rapid increase in radionuclides as explained in the following sections.

2.2 Production of cosmogenic ^{14}C, ^{10}Be and ^{36}Cl

When primary cosmic rays reach Earth and come into contact with the atmosphere, a nuclear cascade is triggered which eventually leads to secondary particles (Masarik & Beer, 1999) such as protons and neutrons. These energetic particles then initiate spallation reactions of atmospheric nitrogen, oxygen and argon - the principal constituents of the atmosphere. These reactions eventually lead to the formation of most cosmogenic radionuclides (Huggle et al., 1996; Yim & Caron, 2006; Beer et al., 2012) with the main reaction pathways detailed herein:

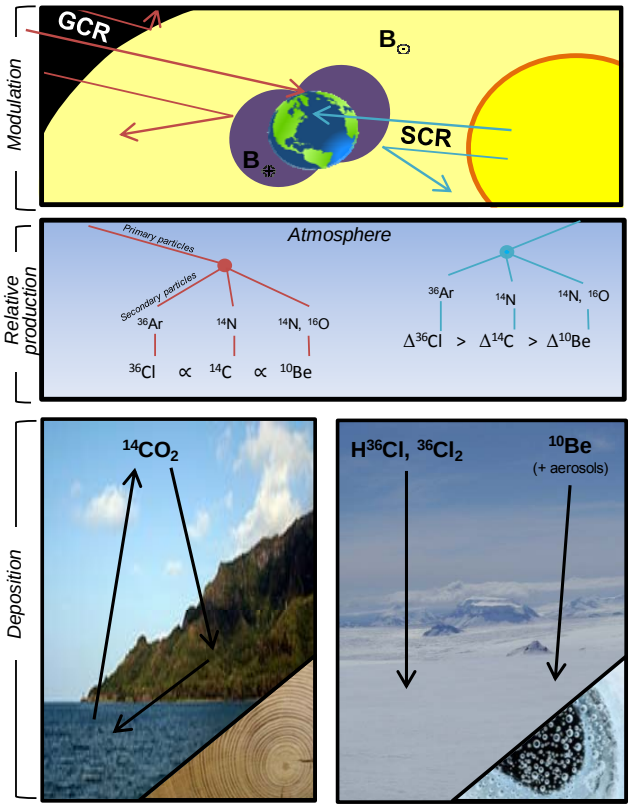

Fig. 2. From cosmic rays to cosmogenic radionuclides. Upper panel : solar and geomagnetic modulation of Galactic (GCR) and Solar (SCR) Cosmic Rays. Yellow shading represents the heliomagnetic field, purple shading represents the geomagnetic field. Middle panel : Relative production of radionuclides in the atmosphere. Primary particles react into secondary particles which through spallation of ^{14}N, ^{16}O and ^{36}Ar creates the relevant radionuclides. Lower panel: deposition processes of ^{14}C, ^{10}Be and ^{36}Cl and related proxies.

$n + {}^{14}N \rightarrow {}^{14}C + p$
$n + {}^{14}N \rightarrow {}^{10}Be + 2n + 3p$
$p + {}^{14}N \rightarrow {}^{10}Be + n + 4p$
$n + {}^{16}O \rightarrow {}^{10}Be + 3n + 4p$
$p + {}^{16}O \rightarrow {}^{10}Be + 2n + 5p$
$p + {}^{36}Ar \rightarrow {}^{36}Cl + 3n + 2$

Carbon-14 chiefly originates from the ^{14}N-capture of neutrons with the reaction emitting one proton. Beryllium-10 results from the nuclear fission of both ^{14}N and ^{16}O caused by secondary neutrons and protons. This requires more energy which is why ^{10}Be is less abundant than ^{14}C. As for chlorine-36, it is the heaviest and rarest radionuclide of the three as it is mainly formed by spallation of ^{40}Ar which accounts for circa 1% of the atmosphere's composition.

The production of cosmogenic radionuclides is latitude and altitude-dependent. Indeed, most production occurs at high latitudes where the geomagnetic field and thus the shielding against cosmic rays is the weakest. As for altitude, radionuclides are mainly produced in the lower stratosphere (65%; Beer et al., 2012) and upper troposphere.

As the middle panel of fig. 2 and fig. 3 depict, cosmogenic ^{14}C, ^{10}Be and ^{36}Cl are differently sensitive to the energy of the incident cosmic rays (Webber et al., 2007). Indeed, the production rates of radionuclides induced from higher-energy GCRs tend to vary proportionally as opposed to solar-induced radionuclides production rates. Figure 3 accordingly evidences that a shift in production pattern happens at the beginning of the solar domain. This is strikingly seen with the abrupt decrease in ^{10}Be production and the leveling of ^{36}Cl which shows that the latter is the more sensitive to lower-energy solar energetic particles (SEPs). It should be mentioned that GCRs

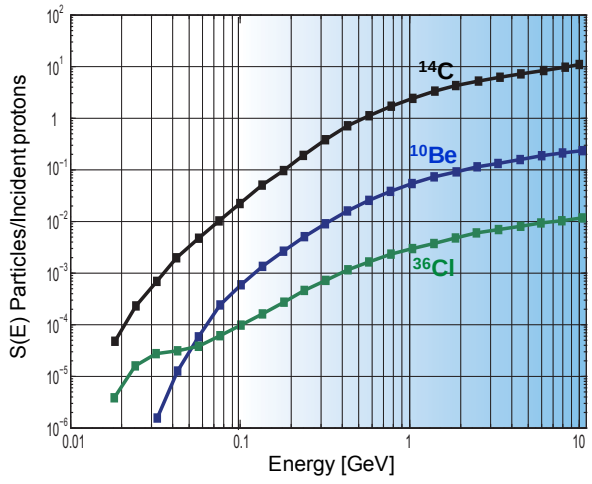

Fig. 3. Yield functions of ^{14}C (Castagnoli & Lal, 1980), ^{10}Be and ^{36}Cl (Webber et al., 2007). Total production in the atmosphere per incident cosmic ray proton as a function of energy. White background represents the solar domain while blue shading represents the galactic domain. Note the shift in production pattern in the solar domain.

make up for most of the radionuclides production on Earth so that the yearly SCRs contribution can appear seemingly negligible. Nevertheless, particularly large solar storms could significantly increase the annual production of ^{36}Cl as compared to ^{14}C and ^{10}Be and as computed for the SEP events of 1960, 1972 and 1989 (Webber et al., 2007). Also worth noting in the light of differences in production processes, is that ^{10}Be is less sensitive to solar modulation than ^{14}C (Muscheler et al., 2007). As a matter of fact, these authors mention that a decrease in solar activity resulting in a 10% increase in ^{10}Be production would yield a ^{14}C increase of 13% (with current geomagnetic field configuration).

To summarize, the formation of cosmogenic radionuclides involves complex nuclear cascades triggered by cosmic rays-induced spallation reactions. Nevertheless cosmogenic ^{14}C, ^{10}Be and ^{36}Cl involve different production processes with different target nuclei (Beer et al., 2012). Hence the involved nuclides have different sensitivities to varying-in-intensity cosmic rays with ^{36}Cl and, to a smaller extent, ^{14}C typically more sensitive than ^{10}Be to lower-energy solar particles. These relative differential production yields of the three radionuclides can thus be used to infer the energy level of incident cosmic rays at a certain point in time.

2.3 Transport and deposition of cosmogenic ^{14}C, ^{10}Be and ^{36}Cl

The three cosmogenic radionuclides used in this study are the most commonly used in galactic and solar irradiation reconstructions. As detailed in §2.2, they vary greatly in terms of energy spectra and production processes. Let us now consider how their transport and deposition mechanisms further differentiate them.

2.3.1 Carbon-14

Carbon-14 ($T_{1/2}$ = 5.73 ka) is the most abundant of the three radionuclides. It also has the longest atmospheric residence time (5 years) due to the carbon cycle. Indeed, when ^{14}C is formed, it can oxidize to atmospheric CO_2 which is taken up by vegetation through photosynthesis. Some of the resulting organic matter eventually decays and oxidizes releasing back CO_2 to the atmosphere although a small portion of it is removed to the soils. Atmospheric $^{14}CO_2$ can also be dissolved in shallow ocean waters where a fraction of oceanic carbon is eventually sequestered to deep ocean waters under the form of $CaCO_3$ (Beer et al., 2012). On geological time scales, some of it eventually returns to the atmosphere through subduction and volcanism. The atmospheric ^{14}C concentration $N_a(t)$ is consequently a function of not only the production rate $Q(t)$ but also the decay $e^{-\lambda t}$ and the carbon cycle $C(\tau)$ as expressed in the following equation (after Beer et al., 2012):

Table 1. Latitudinal deposition of ^{10}Be relative to different atmospheric reservoirs and as a function of latitudinal production (after Heikkilä et al., 2009). Example : 58% of ^{10}Be produced in the troposphere at 30°-60° N is deposited in *situ*, 32% of it is deposited at 0-30° N, 5% is deposited in the arctic, 4% at 0-30° S and finally 1% at 30°-60° S. Blue percentages represent *in situ* deposition.

	Deposition:					
	60°-90° S	**30°-60° S**	**0-30° S**	**0-30° N**	**30°-60° N**	**60°-90° N**
Production *(total):*						
60°-90° S trop. *(2.5%)*	16%	65%	15%	4%	0%	0%
30°-60° S trop. *(6.5%)*	5%	58%	31%	6%	0%	0%
0-30° S trop. *(8.5%)*	1%	17%	58%	21%	3%	0%
0-30° N trop. *(8.5%)*	0%	3%	18%	62%	17%	0%
30°-60° N trop. *(6.5%)*	0%	1%	4%	32%	58%	5%
60°-90° N trop. *(2.5%)*	0%	0%	2%	15%	64%	19%
Stratospheric *(65%)*	2%	23%	24%	24%	25%	2%

$$N_a(t) = \int_0^t Q(t) e^{-\lambda(t-\tau)} C(\tau) d\tau \qquad (1)$$

Carbon-14 can be easily retrieved and accurately dated in tree rings which makes it the most commonly used proxy for solar activity reconstruction (Bard et al., 1997; Usoskin et al., 2003; Muscheler et al., 2007). However, it is important to emphasize that because of its long residence time and complex cycle, ^{14}C content in tree rings does not represent the annual amount of energetic particles reaching the atmosphere but rather a merely damped (Bard et al., 1997) and time-shifted signal of it. This needs to be accounted for using a reversed carbon cycle model which essentially relies on differential equations to describe the exchanges between the different reservoirs and extract the ^{14}C production rate (Siegenthaler, 1983) cf. equation (1). The nature of the carbon cycle also means that ^{14}C content in tree rings represents a well-mixed and global signal. Furthermore, changes in measured radiocarbon content retrieved in tree rings do not necessarily reflect changes of the solar modulation or the geomagnetic field but can also reflect changes in the carbon cycle itself (Muscheler et al., 2005).

2.3.2 Beryllium-10

Beryllium-10 ($T_{1/2}$ = 1.387 Ma), on the other hand is scavenged much more rapidly as it binds to aerosols (Lal & Peters, 1967) and then combines with water droplets which eventually precipitate down to Earth's surface (lower panel fig. 2). Such "wet deposition" is the main removal process of atmospheric ^{10}Be although gravitational settling and dry deposition dominates in desert regions such as Antarctica. Logically, regions characterized by high precipitation rates, namely the tropics and polar fronts, will exhibit the highest wet deposition flux (Heikkilä & Smith., 2013) and fastest scavenging of atmospheric ^{10}Be. Most ^{10}Be is produced in the polar regions but is deposited in latitudes of 30-60°. Despite quick scavenging, ^{10}Be thus represents a more or less hemispherical production signal though to a lesser degree than that of ^{14}C. As a matter of fact, Heikkilä et al. (2009; table 1) found that ^{10}Be produced in the stratosphere (65% of total production) is well mixed and deposited throughout the globe except for the polar regions. As for non-polar tropospheric ^{10}Be, as much as 58-62% is deposited *in situ* with the remaining fraction distributed within the hemisphere of origin. From the table, one can estimate the weight of the different atmospheric reservoirs on the^{10}Be content as archived in polar ice. As such, it is found (Beer et al., 2012) that 60% of ^{10}Be in Greenland is initially produced in the stratosphere while 22% and 18% is produced *in situ* in the troposphere and at 30-60°N respectively. For Antarctica, the numbers are 64%, 20% and 16%. Beryllium-10 produced in the troposphere is very rapidly removed, within a few weeks, and is consequently not as well-mixed as stratospheric ^{10}Be as illustrated in table 1 (Heikkilä et al., 2009). Another difference between ^{14}C and ^{10}Be is that the latter has a less dampened signal than the former and its concentration in annual archives is more closely related to production rate due to its lower residence time ie. 1-2 years (McHargue & Damon, 1991; Masarik & Beer, 1999). Nevertheless, ^{10}Be also has limitations as climate and more precisely atmospheric circulation and precipitation are largely involved in its transport and deposition. Accordingly, ^{10}Be concentration in ice is not only dictated by incident cosmic rays but also by accumulation rates. This can be easily compensated for by calculating the ^{10}Be flux (Berggren et al., 2009). However, this simple calculation only corrects for the accumulation effect and does not consider other potential tempering. Moreover, ^{10}Be is traditionally extracted from ice cores and sediments which have increasing chronology uncertainties with depth/time. This can be very problematic when comparing high resolution ^{14}C and

^{10}Be records as it is the case in this study.

2.3.3 Chlorine-36

Cholrine-36 ($T_{1/2}$ = 301 ka) is less known and used than ^{10}Be and ^{14}C. This is partly due to the fact that ^{36}Cl has very low concentrations so that twice as much ice is needed for AMS measurements than for ^{10}Be. Its transport and deposition mechanisms have consequently been prone to less studies. Once produced from argon, ^{36}Cl is transported and deposited in two ways (Delmas et al., 2004). Similarly to ^{10}Be, ^{36}Cl can attach to aerosols and follow atmospheric circulation pathways, chiefly as NaCl. Also and supposedly more importantly, chlorine is present in the atmosphere as gaseous HCl and Cl_2 where dry and wet deposition would dominate. There still are no robust ^{36}Cl cycle reconstructions which have been attempted. As a result, potential latitudinal dependencies in ^{36}Cl deposition are still unknown. Nevertheless, Synal et al. (1990) have used bomb-produced ^{36}Cl fallouts in order to derive its residence time which they find at 2 years and thus comparable to ^{10}Be. To this day, it can only be assumed that ^{36}Cl as found in ice cores is representative of the production rate. It should be stressed, though, that H^{36}Cl in ice cores is subject to upward diffusion. Indeed, it is believed (Delmas et al., 2004) that during snow metamorphism, a fraction of gaseous HCl is released to the free atmosphere and then deposited back to more modern layers. This unexpected mobility of HCl in ice archives could prove to be problematic for high resolution studies of ^{36}Cl and should be duly noted and taken into consideration.

2.4 Cosmic rays-Climate link

As introduced, the rapid increases in cosmic-rays which occurred at AD 774/5 and AD 992/3 may also have a climatological aspect. Indeed it has been suggested (Svensmark & Friis-Christensen, 1997) that cosmic rays may indirectly force climate by increasing cloud formation. In fact, Ney (1959) and Dickinson (1975) already suggested decades ago the possibility that ionization of cosmic rays in the atmosphere might contribute to cloud nucleation in the vicinity of the tropopause. Theoretically, a decrease of solar activity would lead to a weakening of the shielding and thus an increase of cosmic bombardment on the atmosphere effectively increasing low cloud nucleation and Earth's albedo eventually resulting in a cooler climate. Along those lines, Svensmark & Friis-Christensen (1997) found a statistical correlation between cosmic rays and cloud cover for the years 1984 to 1991. Nevertheless, the latter results were regarded as poorly significant (Jørgensen & Hansen, 2000) due to the low degree of freedom of the correlation (8 points – less than one solar cycle) and due to the very poor understanding of the physical mechanisms of cloud formation. The correlation between cosmic rays and cloud condensation nuclei (CCN) is very intricate because not only cloud cover can be considered but also the microphysical properties of clouds such as cloud droplet size, cloud water content and cloud optical depth (Kristjánsson et al., 2008). Nevertheless the CR-CCN relationship remains an interesting and attractive parameter of the sun-climate link. As a matter of fact, the latter relationship motivated a CERN-directed experiment *Cosmics Leaving Outdoor Droplets* (CLOUD) aiming at better understanding the potential effect of ionizing cosmic radiation on cloud formation. Although the experiment is, to this day, still ongoing it has been found that cosmic rays might in fact substantially increase the nucleation rate of sulphuric acid-ammonia particles (Kirkby et al., 2011). It should be mentioned, though, that as important as this finding is in relation to the potential link between GCR and clouds, uncertainties concerning whether those particles grow sufficiently to seed cloud droplets leave the CR-CCN question open.

The AD 774/5 and AD 992/3 cosmic events could be very interesting to the discussion since they represent the largest outburst of cosmic rays measured to this day. One could thus expect to see an imprint on climate proxies at that time period assuming the CR-CCN link genuine. Similarly, Wagner et al. (2001) investigated the potential link between flux of ^{10}Be and ^{36}Cl at Summit, Greenland with climate proxy data such as δ^{18}O and CH_4. Interestingly, the authors found no correlations between climate and CR-induced radionuclides for the Laschamp event which was marked by a minimum in the geomagnetic field at 36-41.5 ka BP and thus a substantial increase in cosmic rays penetrating Earth's atmosphere casting doubts on a possible link between cosmic rays and climate.

2.5 Solar proton events (SPE)

Since solar proton events are a possible source for the M12 and M13 events and will be discussed in length, a review of their characteristics is needed. Solar proton events, sometimes referred to as solar energetic particle events (when electrons and all nuclides are considered) represent events where the solar proton flux is generally elevated for a few days (Jackman et al., 2005). Some of these particles are accelerated by the sun with sufficient energy to penetrate down to Earth's atmosphere (Shea & Smart, 1990) especially at high latitudes where the geomagnetic field (cutoff rigidities) is weaker.

The intensity of SPEs is typically described by different means which can be somewhat confusing. The most extreme events are often known as ground level events (GLE) which are measured by neutron monitors and defined as % above the pre-event counting rate – such a detection method only captures highly energetic particles. Less energetic solar particles are measured by satellites such as the Geostationary Operational Environmental Satellite (GOES) which provides information on particles

ranging from ~1 to 100 MeV in energy. SPEs can also be described by their specific proton fluence spectrum which represents the amount of particles of different energies (protons) per a surface area (typically cm^{-2}). Two main solar spectra exist – soft and hard. Typically, soft SPEs are characterized by high proton fluxes at low energies (E < 30 MeV) while hard SPEs are characterized by high proton fluxes at high energies (E < 100 MeV). It is believed that soft and hard SPEs originate from different areas in the solar disk (Beer et al., 2012; Cliver et al., 2014). Furthermore, it should be mentioned that it is common practice to refer to the intensity of a SPE by its fluence above 30 MeV ie. F (> 30 MeV) or F_{30}.

Among notable SPEs measured during the instrumental era, we can mention the event of February 1956 which was the strongest and hardest SPE with a GLE peak of 5,500% and a fluence F_{30} of $1.8x10^9$ protons.cm^{-2} (Webber et al., 2007). The highest fluence F_{30} measured belongs to the soft SPE of 1972 with $4x10^9$ protons.cm^{-2}. The largest solar flare, though, is considered to be the Carrington solar flare event of September 1859. Since it occurred prior to the "satellite era", McCracken et al. (2001) used nitrate concentrations archived in polar ice to deduce a fluence > 30 MeV (F_{30}) of ~$1.9x10^{10}$ which is about 5 times more than the SPE of 1972. The Carrington solar flare event is, to this day, considered as the only one to have had a F_{30} in the vicinity of 10^{10} proton.cm^{-2}. Smart et al. (2006) noted that the absence of significant increases in ^{10}Be also archived in polar ice indicates that the solar cosmic radiation produced in the Carrington event had a soft spectrum ie. fundamentally less proton fluences above 100 MeV than above 10 MeV.

Such energetic particles events have the potential to penetrate into and alter the chemistry of the polar atmosphere. As such, many studies (eg. Jackman et al., 1990; Seppälä et al., 2004; Lopez-Puertas et al., 2005) have reported enhancements of nitric and hydrogen oxides and depletion of ozone which can potentially affect surface air temperatures (Callisto et al., 2013).

3 Methods & Dataset

In order to estimate the origin of the two events, several records of ice core ^{10}Be and ^{36}Cl as well as tree rings ^{14}C have been used. As for investigating a potential impact on the atmosphere, several proxy records found in ice cores have been used. The resulting dataset (table 2) and analytical methods are described in the following section.

3.1 Available data

3.1.1 Cosmogenic radionuclides records

There exist two ice cores (GRIP and Dome Fuji) for which ^{10}Be and/or ^{36}Cl have been measured during the relevant periods (the 8th and 10th centuries). Beryllium-10 is available at quasi-biannual resolution from the GRIP ice core (Muscheler et al., 2004; Vonmoos et al., 2006) but many results are still lacking engendering a very erratic record as evidenced by fig. 4. In addition to ^{10}Be, ^{36}Cl is also available though at lower resolution (fig. 4). Indeed, two samples were combined as the lower concentration of ^{36}Cl in ice would otherwise not allow for reliable measurements. Despite the lack of many samples and the resolution of 5 years, this record is genuinely important because of the sensitivity of the ^{36}Cl production rate to low energy particles. As for Dome Fuji (fig. 4), the Antarctic record displays ^{10}Be concentrations with unequidistant resolution ranging from 10 to 15 years.

Regarding ^{14}C, the IntCal13 calibration curve (Reimer et al., 2013) represents a good continuous record allowing one to investigate radiocarbon fluctuations as well as solar activity throughout the Holocene and beyond. The calibration curve utilizes Δ^{14}C measurements from tree rings. The smoothed aspect of IntCal13 is not optimal to compare the enrichment in ^{14}C to its other radionuclide counterparts which is why the annual to biannual Δ^{14}C measurements of Miyake et al. (2012, 2013), displayed in fig. 1, were used for the subsequent analysis.

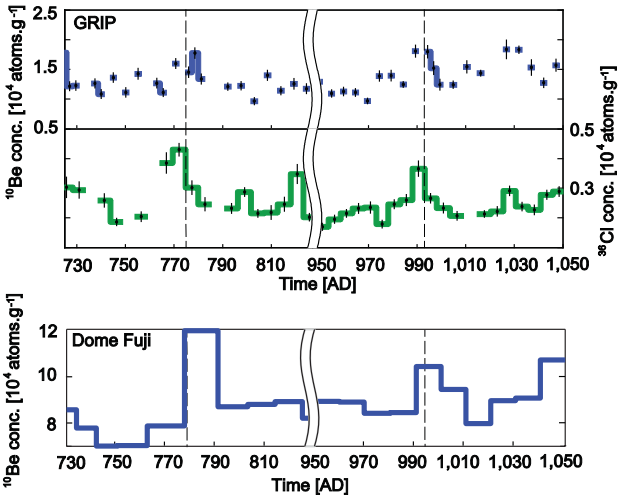

Fig. 4. GRIP (Wagner et al., 2000; Muscheler et al., 2004; Vonmoos et al. 2006) and Dome Fuji (Horiuchi et al., 2008)) ^{10}Be and ^{36}Cl records at the relevant periods. Note the break in the timescale between AD 826—949 placed to ease visualization. Dotted lines represent expected occurence of the two cosmic events.

Table 2. Ice core and tree rings proxy records used and characteristics. Res.= Resolution, CFA=Continuous Flow Analysis data, atm. circ.=atmospheric circulation.

Record	**Source**	**Proxy** (for)	**Time span** [AD]	**Res.** [years]	**Investigator**
IntCal13	tree rings	^{14}C (cosmic rays)	<0 – 1950	1-10	Struiver et al., 1998
					Reimer et al., 2013
Japanese Cedars	tree rings	^{14}C (cosmic rays)	770 – 800	1 -2	Miyake et al., 2012
			988 – 1018	1 - 2	Miyake et al., 2013
Crete	ice Greenland	δ^{18}O (climate)	554 – 1278	<0.1	Clausen et al., 1988
Dome Fuji	ice Antarctica	^{10}Be (cosmic rays)	699 – 1876	10 -15	Horiuchi et al., 2008
Dye 3	ice Greenland	δ^{18}O (climate)	<0 – 1872	1	Vinther et al., 2006
GRIP	ice Greenland	δ^{18}O (climate)	551 – 1979	1	Vinther et al., 2006
		^{10}Be (cosmic rays)	<0 – 1645	2.5	Muscheler et al., 2004
					Vonmoos et al., 2006
		^{36}Cl (cosmic rays)	<0 – 1645	5	Wagner et al., 2000
NGRIP	ice Greenland	δ^{18}O (climate)	0 – 1995	1	Vinther et al., 2006
		CFA (atm. circ.)	743 – 1002	<0.1	McConnell (pers.comm.)
		^{10}Be (cosmic rays)	765 – 792	1	This study
			985 – 1015	1	This study

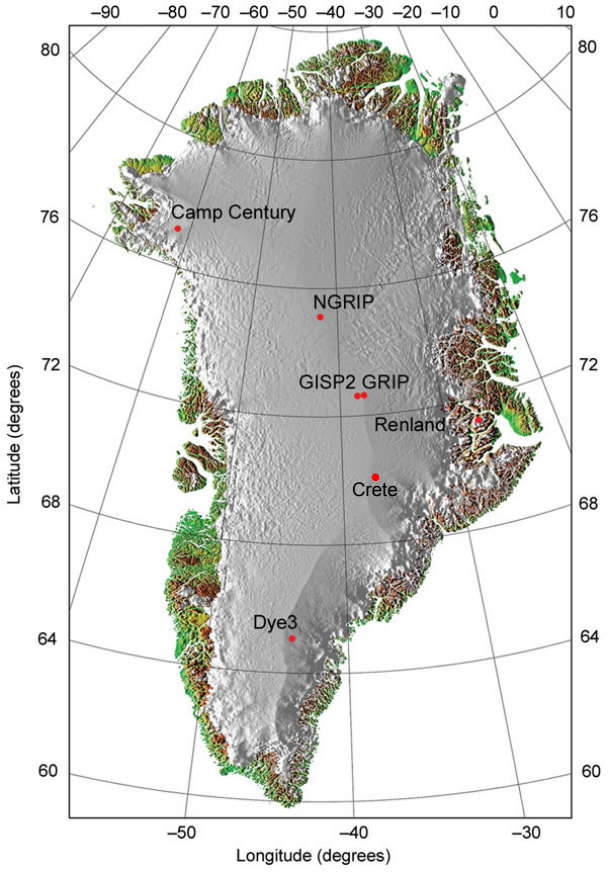

Fig. 5. Location of Greenland ice cores (modified from NGRIP members., 2004; originally provided by S. Eckholm, Danish Cadastre). Note the N-S geographical spread of NGRIP, GRIP, Crete and Dye 3.

3.1.2 Glaciochemical data

To link such rapid increases in cosmic radiation to climate, it is crucial to have very high resolution climate records in geological archives. Regrettably, very few annually resolved climate proxies (eg. ice cores, tree rings, sediments and chironomids in varves, speleothems) are available for the relevant periods. Indeed, too few tree chronologies exist to allow for a statistically thorough reconstruction while annually laminated sediments and speleothems are very scarce. As a result, this paleoclimatic investigation is merely a Greenland atmospheric reconstruction with several ice core proxies used as detailed in table 2. There exist 4 ice cores with annually resolved δ^{18}O data at the time period of the 2 events: Dye 3, the Greenland Ice Core Project (GRIP), Crete and NorthGRIP. As evidenced in fig. 5, the spatial distribution of the latter ice cores span across the whole of Greenland, on a N-S perspective. This fact is important because it would allow one to extract a regional signal (Vinther et al., 2003).

In addition, unpublished dust/gaseous impurities measurements from the NGRIP ice core provided by McConnell et al. have been used in order to estimate changes in atmospheric circulation patterns. The extensive data have been extracted utilizing continuous flow analysis (CFA). This method

consists in continuously melting sections of an ice core supplying a sample water flow which is then analyzed (Kaufmann et al., 2008). CFA allows for very high resolution with lower risks of contamination bias as only the inner part of ice core sections is analyzed. The NGRIP record used herein consists of a multitude of dissolved and particulate impurities as detailed in table 3.

Table 3. List of all impurities in the NGRIP CFA data provided by McConnell et al. (pers. comm.).

Elements, chemical compounds and ions	Symbol
hydrogen peroxide	H_2O_2
ammonium	NH_4^+
nitric acid	HNO_3
$\delta^{18}O$	$\delta^{18}O$
black carbon	bC
magnesium	Mg
sulfur	S
non-sea salt sulfur	nssS
calcium ion	Ca^{2+}
non-sea salt calcium	nssCa
manganese	Mn
sodium	Na
rubidium	Rb
strontium	Sr
cadium	Cd
lanthanum	La
cerium	Ce
thalium	Tl
lead	Pb

3.2 NorthGRIP ^{10}Be

Figure 4 strikingly shows that the existing ^{10}Be and ^{36}Cl ice core records are not optimal for this study which requires continuous data at high resolution. This motivated the acquisition of new and annually resolved ^{10}Be data obtained from the NGRIP ice core.

3.2.1 Ice sampling

The NGRIP ice core samples were retrieved from the Centre for Ice and Climate in the Niels Bohr Institute of the University of Copenhagen, Denmark. The ice core was initially cut into 55cm segments (fig. 6-A) in situ at the coring site in Greenland. In order to ensure high resolution measurements each bag was cut with a band saw into 3 samples inside the freezer which should correspond to annual resolution. The resulting 57 ice samples were then transported to the Beryllium-10 laboratory at the Geoscience Department of Uppsala University, Sweden for preparation for Accelerator Mass Spectrometry (AMS) measurements of ^{10}Be.

3.2.2 Chemical preparation for AMS measurements

The chemical preparation of 10Be described henceforth follows the same procedure than that of Berggren (2009). To begin with, the ice samples of 100-170g were cleaned with deionized and distilled water to eliminate potential contamination such as drilling fluid and/or handling. Two solutions of 1 mL 0.103 ppmw µg/ml standard Beryllium (^{9}Be-carrier) and 4 mL 998.2-1019.9 ppmw µgCl/g (^{35}Cl-carrier) were then precisely added to the ice using a digital pipette. The ^{9}Be-carrier is needed in perspective of the AMS measurements to estimate the ^{10}Be/^{9}Be ratio and subsequently calculate the amount of ^{10}Be present in each sample. As for the ^{35}Cl-carrier, it was added in regard of the same purpose. That is, of eventually calculating the amount of ^{36}Cl although this will be measured in further studies and will thus not be included herein. Introducing the carriers as early as possible in the procedure is vital because, in case of loss of material, the ratio would remain constant and thus the AMS measurements unbiased. The next step in the preparation was to melt the ice samples using a microwave oven. This was done using short increments of time so that the samples would not warm excessively.

The melted samples were poured into drip bags themselves linked to cation exchange columns (Bio-Rad Poly-Prep® prefilled chromatography cation columns AG 50W-X8 resin 100-200 mesh hydrogen form 0.8x4 cm), via silicon tubes (fig. 6-B), which are aimed at capturing the ^{9}Be and ^{10}Be from the water. The residual water was then directed to anion exchange columns (manually filled with Bio-Rad AG® 4x4 resin 100-200 mesh free base form) in order to retain ^{36}Cl and its related carrier, ^{35}Cl. As depicted in fig. 6-B, the samples were combined by two for the Cl columns to ensure the feasibility of AMS measurements as concentration in ice of the latter isotopes is even lower than that of berylluim. It should be mentioned that several blanks consisting of circa 150g of distilled and deionized water were processed in the same manner which would ultimately allow for an estimation of the background noise.

The beryllium resins were subsequently eluted (fig. 6-C) by mounting open quartz tubes on top of the columns and pouring in 25mL of 4 M HCl. The resulting fluid, the eluate, consists of the acid and the beryllium isotopes. 12 mL of ammonia (NH_3) was then added to the eluate in order to raise the pH between 6 and 12 and thus obtain a basic solution so that beryllium hydroxide would form. The samples, placed

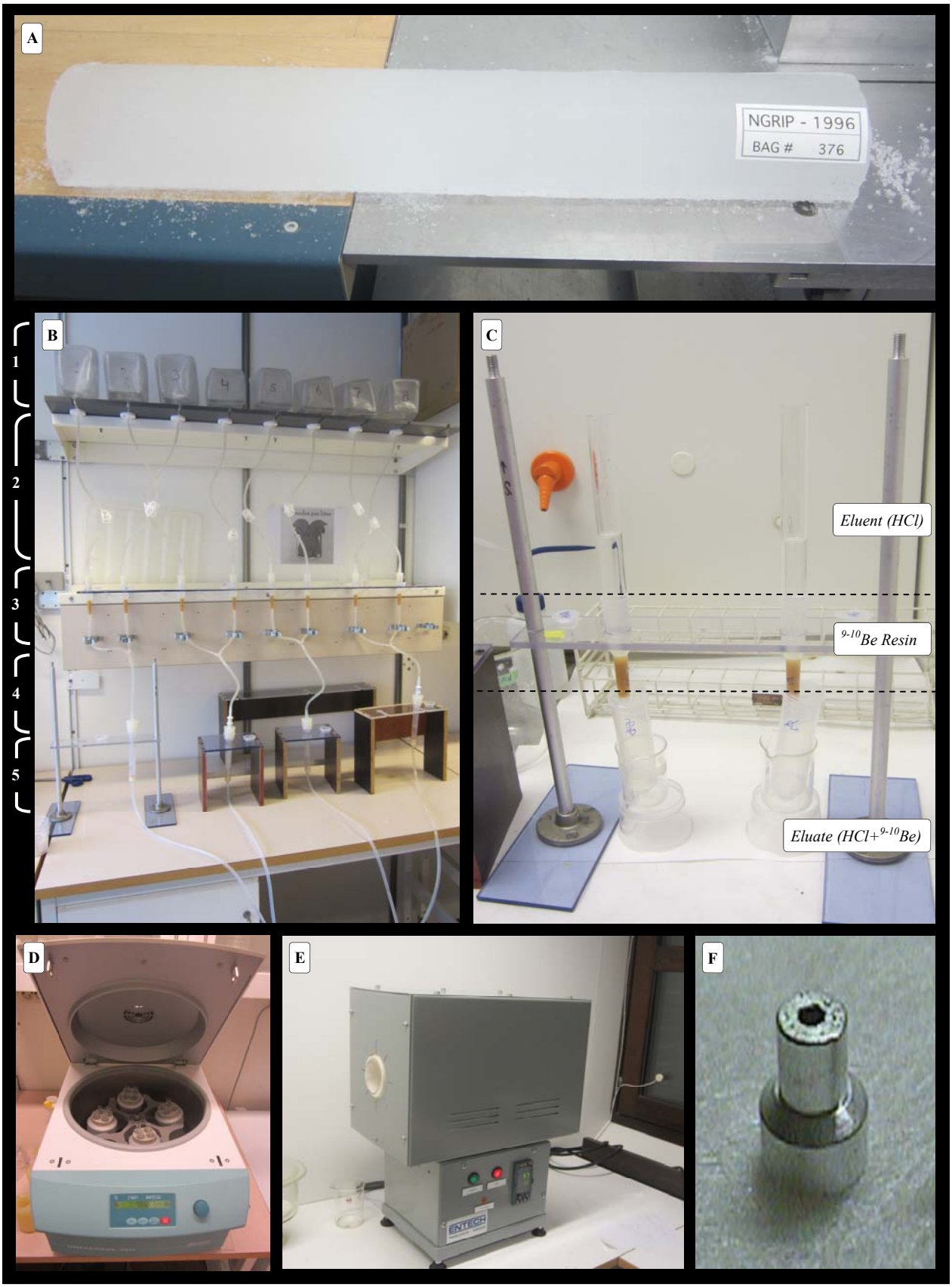

Fig. 6. Panel depicting the different stages of the ^{10}Be sampling, preparation and measuring. A) A NGRIP bag before sampling at annual resolution. B) ^{10}Be extraction : 1. Drip bags with water samples - 2. Silicon tubes 3. Cation exchange columns for Beryllium - 4. Combining 2 samples for ^{36}Cl - 5. Anion exchange columns for ^{36}Cl. C) Elution of Be columns. D) Centrifuge used to separate $Be(OH)_2$ from $HCl+NH_3$ and water. E) Furnace used to oxidize samples to BeO. F) Example of cathodes with pressed $^{9\text{-}10}$BeO+Nb placed in AMS holders.

in centrifuge tubes, were then left covered overnight to maximize the precipitation of $Be(OH)_2$. The samples were then centrifuged (fig. 6-D) at 5000 RPM for 20 minutes in order to separate the $Be(OH)_2$ precipitate, agglutinating as a translucent gel at the bottom of the tubes, from the residual solution. The gel-like $Be(OH)_2$ was thereafter transferred to small centrifuge quartz tubes into which distilled and deionized water was added. After stirring thoroughly the water and the precipitate, the quartz tubes were centrifuged – this two-step cleaning procedure was repeated four times. Eventually, the water was discarded and all that remained was the $Be(OH)_2$ gel.

The samples could subsequently be placed and heated in a (ENTECH 1400W ETF 70/12-Spec) furnace (fig. 6-E). During the first hours, the heat was incrementally raised to 60°C to prevent boiling and thus loss of beryllium. Then, the samples were gradually heated to 150°C for 30 minutes and kept at that temperature for 2 hours to make them utterly dry. In order to form beryllium-oxide (BeO), the heat was slowly (ie. over a span of 2 hours) raised to 850°C and kept at this temperature for another 2 hours. The temperature was then decreased gradually for the samples to cool down to circa 100°C, at which point they were placed into an exsiccator to prevent air moisture to come into contact with them before the pressing procedure.

Once the powder-like BeO had reached room temperature, about 1 mg of niobium (Nb) was added to the samples, in the quartz tubes, to facilitate AMS measurements. The BeO-Nb mixture could then be pressed into cathodes (fig, 6-F) in which another mg of Nb was added before sealing them with an aluminum wire.

It should be mentioned that every tool and recipient used were thoroughly cleaned in particular manner as detailed in fig. 7 which displays every step of the chemical preparation.

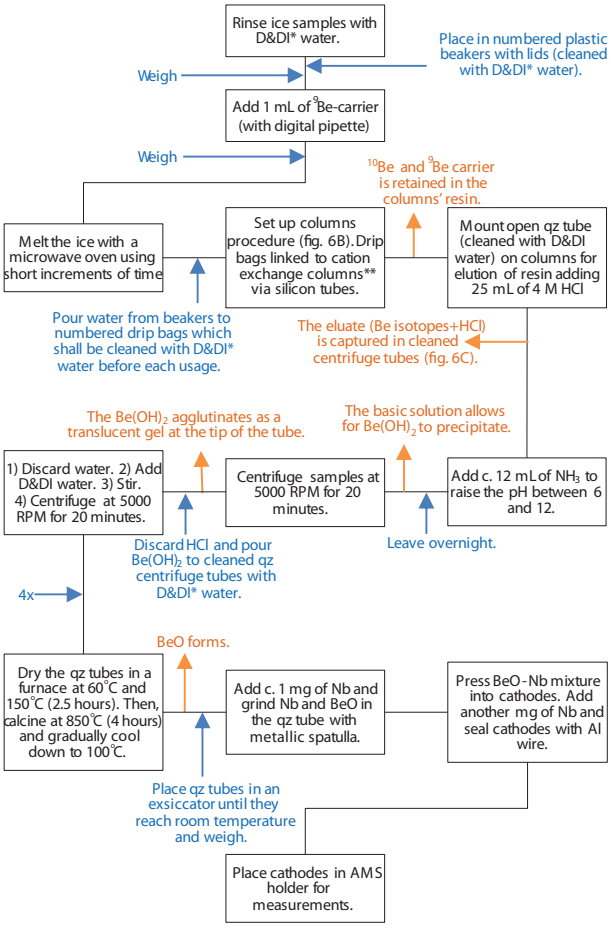

Fig. 7. Flowchart for ^{10}Be chemical preparation. The boxes represent the different steps of the procedure. Blue text represent additional information while orange text represents effect of preceding box.*Distilled and Deionized **Bio-Rad Poly-Prep® prefilled chromatography cation columns AG 50W-X8 resin 100-200 mesh hydrogen form 0.8x4 cm)

3.3 Data treatment and analysis

3.3.1 Background level

The production of cosmogenic radionuclides is strongly dictated by incident galactic cosmic rays with other contributions such as solar protons and supernovae-induced gamma-rays fairly negligible. Nevertheless, it has been computed (Webber et al., 2007) that particularly large SPEs can lead to noticeable enhancements in ^{10}Be and ^{36}Cl yearly production. As a matter of fact, these authors found 13 instrumental SPEs in the last half century which are expected to have had an impact on ^{10}Be and ^{36}Cl production rate. In the case of the M12 and M13 events, though, the paradigm is inverted with the peaking production expected to echo abnormal outbursts of solar protons or gamma-rays rather than ordinary galactic cosmic rays (Miyake et al., 2012). To approximately know how many nuclides have been generated by the events and thus the energy level of their origin, one must separate both signals.

To do so, the production induced by galactic cosmic rays must be estimated and subtracted from the total amount of radionuclides in the records which would give the baseline of the peaks. Cosmic rays are modulated by solar activity and the geomagnetic field as detailed in §2.2.

For ^{14}C, IntCal13-based production rate curve could appear as a candidate of choice to represent the background level of radiocarbon prior to the events. However, the dataset is influenced by the ^{14}C spikes themselves (fig. 8) resulting in an underestimation of

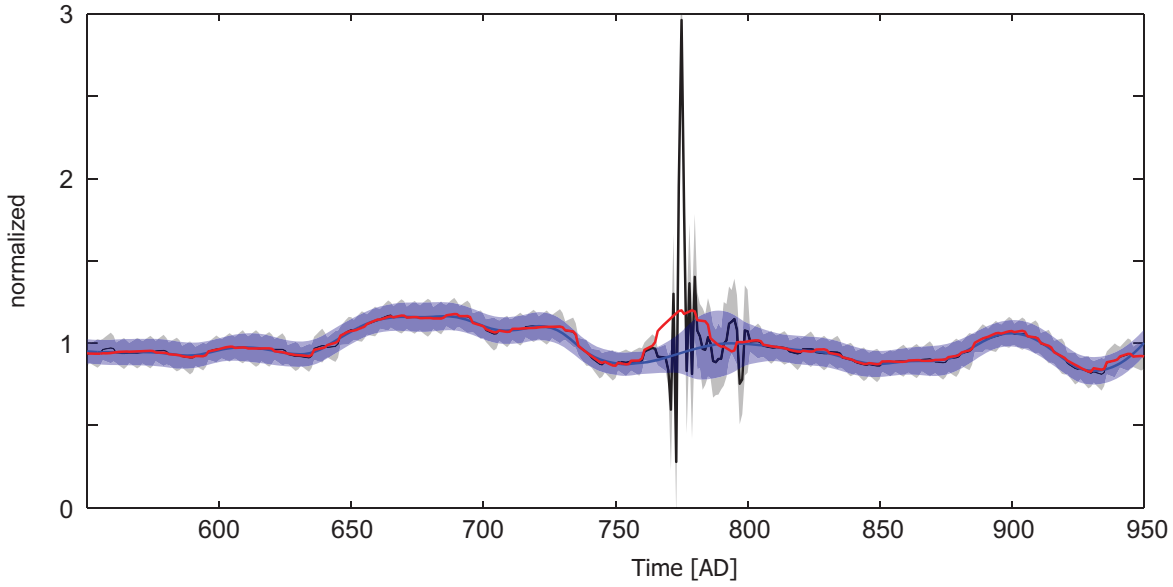

Fig. 8. Example of two potential background levels of radiocarbon. ^{14}C production rate based on Intcal13 and Miyake et al. (2012) data is in black with grey shading representing error margins. Procuction rate based on IntCal13 is represented in red. As for the blue curve, it depicts a robust least-squares regression applied to the ^{14}C production rate. Note that the main discrepency between IntCal13 and the regression method appears at the M12 event.

solar activity and ergo an underestimation of ^{14}C production caused by the cosmic outbursts. In order to obtain an undistorted and reliable ^{14}C background level, a smoothing function robust against outliers was applied to the 14C production rate based on IntCal 13 and Miyake et al. (2012; 2013) data. The function consists of a local regression which assigns zero weight to data outside six mean absolute deviations. As it can be seen in fig. 8, the main discrepancy arises from the time period of the peak. One can observe that the IntCal13 production rate (red curve) is forced towards higher values around AD 774/5 as opposed to the robust local regression (blue curve) which rather represent the bulk behaviour of the neighbouring data of the peak describing a small solar minimum. Another potential choice for the ^{14}C background would be to use the mean pre-industrial production rate as did Usoskin et al. (2013). Though, it should be mentioned that the latter method could either over- or under-estimate the peak amplitude if it would be occurring during a solar maximum or minimum respectively.

In the light of those arguments, applying a robust local least-squares smoothing to the ^{14}C data represents the most suitable and reliable estimation of the background level of the latter radionuclide. Indeed, this method presents the advantage of both representing a good averaged trend and of being robust against outliers. The same logic has been applied to the ^{36}Cl data.

As for ^{10}Be, the scarce number of data points (ie. 27 and 30) does not allow for a relevant local regression to be applied. As a consequence, the background level will be defined as the average value of ^{10}Be prior to and following both events.

3.3.2 Deposition fluxes and production rates

Radionuclides archived in ice cores are measured as concentrations expressed in atoms/g_{ice} so that more precipitation is expected to dilute concentrations (Berggren et al., 2009). As a result, ^{10}Be and ^{36}Cl fluxes were calculated as below:

$$F = \frac{A * \rho_{ice} * C}{S} \quad (2)$$

where A is the accumulation rate in cm/year, ρ_{ice} is the density of ice in g/cm^3, C is the measured concentrations in atoms/g and S is the number of seconds in a year. As such, fluxes are expressed in atoms/cm^2/second. In addition, fluxes or production rates are needed to have a quantitative appreciation of the supplementary production caused by the cosmic events.

As for $\Delta^{14}C$, carbon cycle modeling was needed to obtain the production rate record as explained in §2.3. The model used was programmed in MatLab Simulink (Muscheler, 2000) and is based on the outcrop-diffusion model of Siegenthaler (1983). Such models are not designed for the investigation of abrupt and yearly changes in atmospheric carbon content which is why several low pass filters have been tested. The radiocarbon production rates were calculated as normalized values. As a result, the values were multiplied by 2.02 which is considered as the

global pre-industrial ^{14}C production rate in atoms cm^{-1} s^{-1} (Masarik & Beer, 1999).

3.3.3 Yield functions and response functions

Since relative cosmogenic production is directly depending on the energy of cosmic particles, one can deduce the energy domain of a particular event by comparing the relative production increases of various radionuclides. To do so, the yield functions of Webber et al. (2007) have been used. Yield functions represent the total production of various cosmogenic isotopes in the atmosphere per incident particles as a function of energy (Webber et al., 2007) as shown in fig. 3. These functions were mathematically obtained using the FLUKA code (Fasso et al., 2001), which uses a Monte Carlo calculation of atmospheric production of cosmogenic radionuclides. The energy range of these functions spans from 10MeV to 10GeV which perfectly suits this study as it covers solar as well as galactic cosmic-rays energy domain.

While the use of yield functions allows for an estimation of the energy level of the events, it does not provide a clear picture of the fluence of the events. To this end, response functions have been used. These functions are expressed as follow (Beer et al., 2012):

$$R(E,t) = J(E,t) * S(E) \quad (3)$$

where *J(E,t)* is the differential spectrum of cosmic radiation (eg. solar particles or gamma-rays) and *S(E)* is the specific yield function. As a result, response functions could help one to estimate the fluence of the events given that production of radionuclides during the M12 and M13 events are known and that the energy spectrum is assumed.

3.3.4 Principal Component Analysis

The NorthGRIP CFA data provided by McConnell et al. represents a remarkable window into the Arctic atmospheric circulation and composition throughout the M12 and M13 events at quasi-monthly resolution. The rather extensive dataset is at the same time hard to visually interpret owing to the many variables and seasonal cycles. Most of these variables are nevertheless driven by common forcing agents and consequently display similar bulk behavior. For this reason, principal component analysis (PCA) has been applied to the data. PCA allows for generating a new set of variables – the principal components - by detecting linear dependencies between variables and replacing groups of correlated variables by new uncorrelated variables (Trauth, 2007). The first Principal component PC1 and associated first eigenvector λ_1 contain the most of the variance with subsequent principal components and eigenvectors characterized by decreasing explained variance. (Trauth, 2007).

Furthermore, high resolution investigation of high frequency climate data such as $\delta^{18}O$ can be very difficult because of the possibility of bias from noise. Such noise is commonly locally induced ie. wind ablation or diffusion. As a result, PCA has also been applied in order to single out such noise and isolate a common regional Greenland $\delta^{18}O$ signal (Vinther et al., 2003). Indeed the four ice cores used are very distant in location (fig. 5) providing a Northern signal (NGRIP) a central signal (Crete and GRIP) and a southern signal (Dye 3). The period chosen for the $\delta^{18}O$ analysis was AD 553-1100, the lower limit being the earliest common data. Furthermore, PCA has been applied to 4 red noise series in order to estimate the amount of noise in the PC1 and $\delta^{18}O$ records.

3.3.5 Estimating significance with the Montecarlo approach

Correlation coefficients can sometimes convey a biased view on the relationship between two time series because they do not consider the likelihood of a match. For instance, if two smoothed series are compared, they may appear seemingly well-correlated though the level of significance would be low because of the high probabilities of having such a match by chance increase with increasing autocorrelation. In that light, Montecarlo simulation has been performed on every relevant correlation coefficient measured. To do so, a red noise series was computed taking in consideration the spectral properties and the autoregressive characteristics of the time series investigated eg. $\delta^{18}O$. This was done iteratively 10,000 times. The derived series were then correlated to the "cause series" (the annually-resolved ^{10}Be or ^{14}C measurements in this study) in order to test the null hypothesis and to estimate the significance of the initial correlation coefficient.

3.3.6 Wavelet analysis

The analysis of the $\delta^{18}O$ time series was also complemented by wavelet transforms as an additional tool for significance testing. Indeed, time series derived from climate proxies are often characterized by intermittent oscillations and wavelet transforms are commonly used to analyze such data which contain non-stationary power at several frequencies

(Daubechies, 1990). In this study, the wavelet transforms were used as a check, in order to assess whether potential correlations between the M12 and M13 events and the climate proxies depict causality or are simply an artifact from an intermittent high frequency oscillation.

4 Results

4.1 The events as recorded in radionuclide records

4.1.1 New NGRIP ^{10}Be measurements

The new annually-resolved NGRIP ^{10}Be data from this study (fig. 9) span over the time periods AD 765-792 and AD 985-1015, based on the Greenland Ice Core Chronology 2005 (GICC05; Vinther et al., 2006). One can readily distinguish an excursion at AD 768-9 reaching concentrations of 4.72 10^4 atoms/g and lasting 3-4 years. This consequently confirms the rapid increase in Δ^{14}C discovered by Miyake et al. (2012) providing yet another independent record displaying the related event. Furthermore, this proves the global aspect of the M12 event (AD 774/5) as it is recorded in ice ^{10}Be in both the Arctic (NGRIP) and likely the Antarctic (Dome Fuji; fig. 4). Intriguingly the spike, as recorded in the new NGRIP ^{10}Be data, is shown to occur 7 years earlier than expected which is discussed in §5.4. As for the M13 event (AD 992/3), ^{10}Be concentrations do not exhibit a proportionally comparable spike to its 8th century counterpart though one can observe two excursions at AD 988.5-989.5 and AD 1000.

The measured ^{10}Be flux nevertheless gives clues as to which excursion is related to the proposed late-10th century event. Indeed and as depicted in fig. 9, ^{10}Be flux shows higher values for the AD 988.5-985.5 spike and inversely lower values for the AD 1000 spike. Furthermore, the latter excursion is composed of only 1 data point as opposed to the former which could advocate for it simply being noise, perhaps induced by weather (Muscheler & Beer, 2006). This implies that the M13 event is recorded earlier than expected in the NGRIP ice core too, though with a shift of 4-5 years. The occurrence of an excursion also confirms the existence and the likely global aspect of the M13 event. The two mentioned excursions apart, the ^{10}Be flux shows to correlate well with ^{10}Be concentrations with the values ranging within errors.

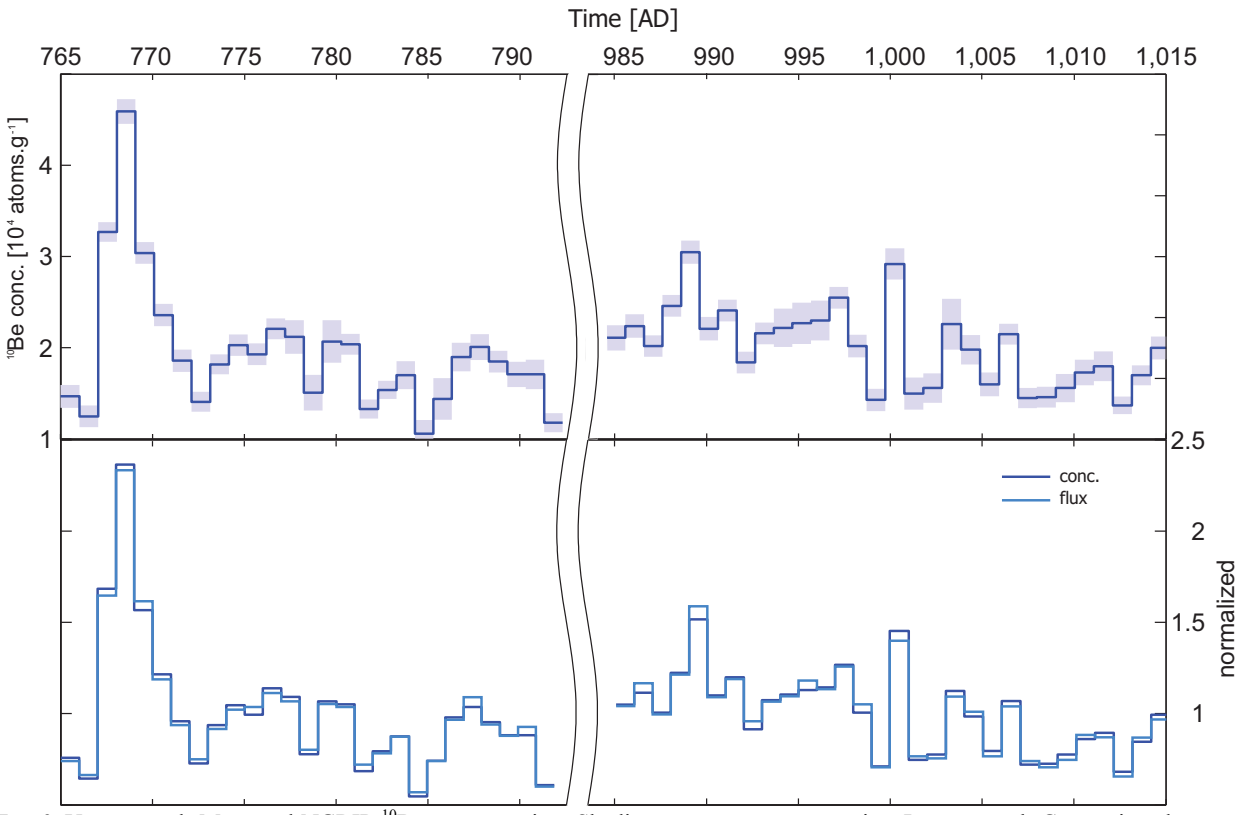

Fig. 9. Upper panel: Measured NGRIP ^{10}Be concentration. Shading represent error margins. Lower panel: Comparison between measured ^{10}Be concentration and calculated ^{10}Be flux. Note the break in the timescale between AD 796—984 placed to ease visualization

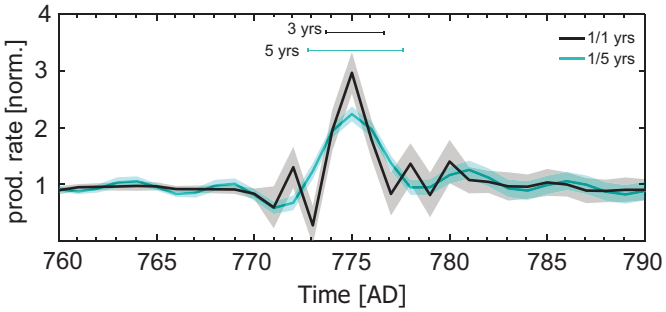

Fig. 10. Comparison of lowpass-filtered series with a cutoff frequency of 1/5 years^{-1}.

4.1.2 ^{14}C production rate

Figure 10 displays the modeled production rate for radiocarbon during the M12 event based on the Δ^{14}C from Miyake et al. (2012). It exhibits that lowpass-filtered records with a cutoff frequency of both 1/5 years^{-1} and 1/1 years^{-1} are altogether similar. The main discrepancy is observed at the time period of the AD 774/5 peak. As a matter of fact, the 1/1-year curve is better constrained in time and its peak is higher in amplitude albeit featuring oscillations prior to and following it. On the other hand, the 1/5-years curve is expectedly smoother which results in the peak being damped in amplitude and less constrained in time although it does not feature strong oscillations. It should be mentioned that both curves are equally correlated to the NGRIP ^{10}Be data with r^2=0.86. In this study, the production surplus associated with the two events, M12 and M13, is a key variable. With this in mind, the lowpass-filtered series with a cutoff frequency of 1/1 year^{-1} is regarded as better suited because it is better constrained in time, has a more realistic peak amplitude as the input data is not smoothed and because its only drawback, the oscillations, are of no real impact.

4.1.3 Production surplus

The M12 event (AD 774/5) - Having defined the background levels of each radionuclide records, one can compare the amplitude and aspect of their signature increases. Both the NGRIP ^{10}Be flux and the modeled ^{14}C production rate show that the M12 event-related peak is constrained within 3 years (fig. 11a). With such an increase of 3 years in production-deposition and a background level calculated at 1.54 atoms.cm^{-2}s^{-1}, it is found that ^{14}C production induced by the M12 event increased by a factor of 3.98 spread over 3 years. As for ^{10}Be flux, the background level was estimated at 0.0102 atoms.cm^{-2}s^{-1}. As a result, it is found that ^{10}Be production increased similarly to ^{14}C with a factor of 3.25 also spread over 3 years. The NGRIP ^{10}Be flux interestingly features a somewhat sinusoidal variation with a frequency of about 1/11 years which is in accordance with solar modulation related to the 11-years cycle. A sine wave function of such frequency is plotted in fig. 11a in order to better illustrate this phenomenon which also shows that the event possibly occurred during the low phase of a solar 11-years cycle. Finally, the background level of ^{36}Cl was placed at 0.0017 atoms.cm^{-2}s^{-1}. Estimating the production surplus in ^{36}Cl is somewhat more complicated because of the poor resolution of the GRIP record. Moreover, one can see (fig. 11a) that the peak as recorded in Greenland ice cores (AD 767-769) is split into two 5-years samples in the GRIP ^{36}Cl record thus further dampening the amplitude. With concern for thoroughness, a minimal and maximal peak has been estimated with the mean value displayed in the figure. The minimal value of 0.0035 atoms.cm^{-2}s^{-1} is based on the assumption that the background level is better represented by the inferred solar modulation, which is shown in fig. 11a, and by only considering the higher peak ie. AD 769-774. Conversely, the maximal value of 0.0055 atoms.cm^{-2}s^{-1} is based on the initially estimated background level and by considering both peaks ie. AD 764-769 and 769-774. By doing so, it is found that ^{36}Cl increased by a factor of 5.12 ± 1.75 spread over 3 years during the M12 event.

The M13 event (AD 992/3) – The M13 event yielded substantially shorter peaks in radionuclides production constrained within two years as evidenced in fig. 11b. The production surplus in radiocarbon caused by the event is found to be of a factor of 1.87 as compared to a calculated background level (§3.3.1) of 1.63 atoms.cm^{-2}s^{-1}. With a background level of 0.0102 atoms.cm^{-2}s^{-1}, the ^{10}Be flux shows an enhancement in production by a factor of 0.88. It is also interesting noting that the ^{10}Be record is noisier than its 8th century counterpart and does not display any clear cycles. On the other hand, the chlorine-36 concentrations show a clearer and single 5-years peak corresponding to the event. Nevertheless, the high values in ^{10}Be prior to and following the event cast doubts on the assumed background level which would directly affect the assumed 2-years peak responsible for the ^{36}Cl M13 event sample high value. As a result, realistic minimal and maximal peaks were once again estimated and displayed in fig. 11b. The maximal value of 0.0036 atoms.cm^{-2}s^{-1} assumes that the 5-years increase in ^{36}Cl is fully caused by the 2-years peak and that the remaining 3 years are composed of concentrations averaging the background level. On the other hand, the minimal value of 0.0029 atoms.cm^{-2}s^{-1}

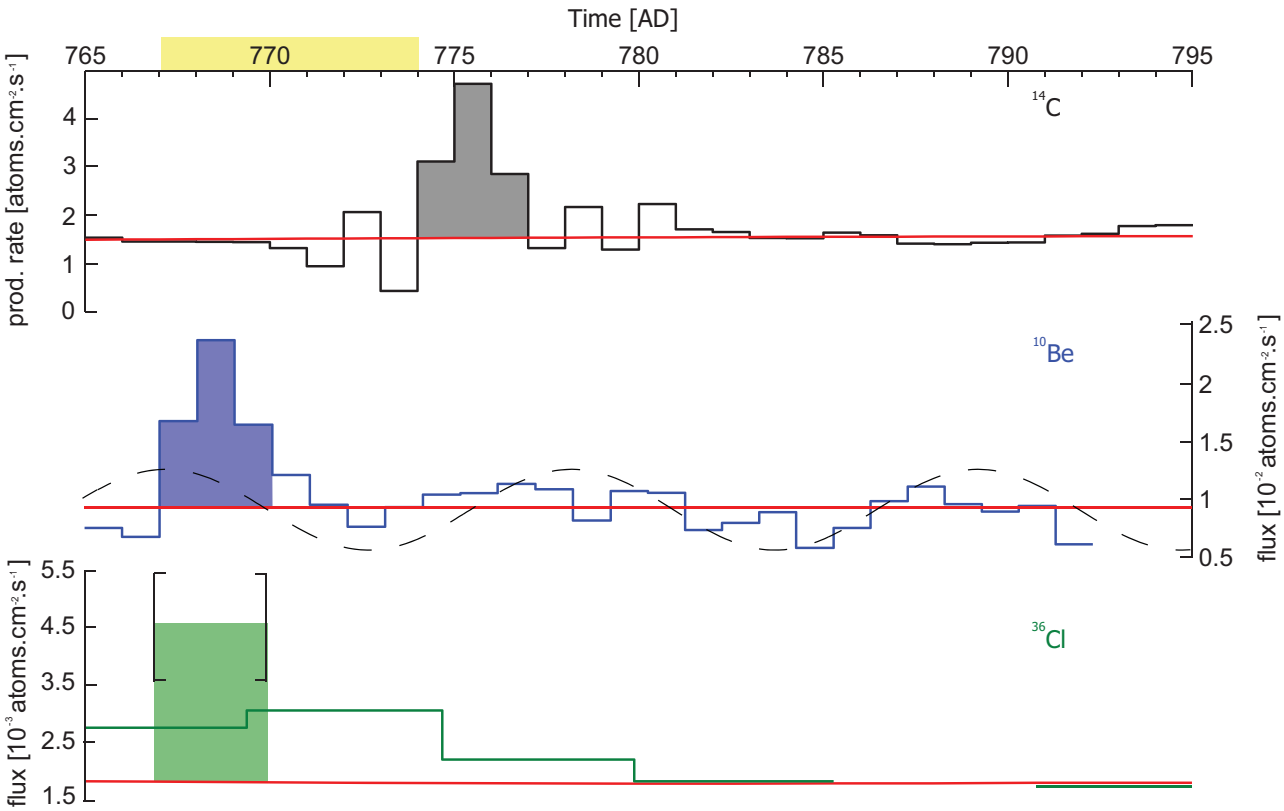

Fig. 11a. Surplus of radionuclides production and fluxes induced by the M12 event (AD 774/5). Red curves represent background levels, shadings represent production surplus, the dashed curve represents a sine wave function with a frequency of 1/11 years related to the solar 11-years cycle. Error bars in ^{36}Cl production arise from uncertainties and assumptions caused by the poor resolution. The yellow shading on the x axis emphasizes the chronology difference between the tree ring counting and the GICC05 time scales.

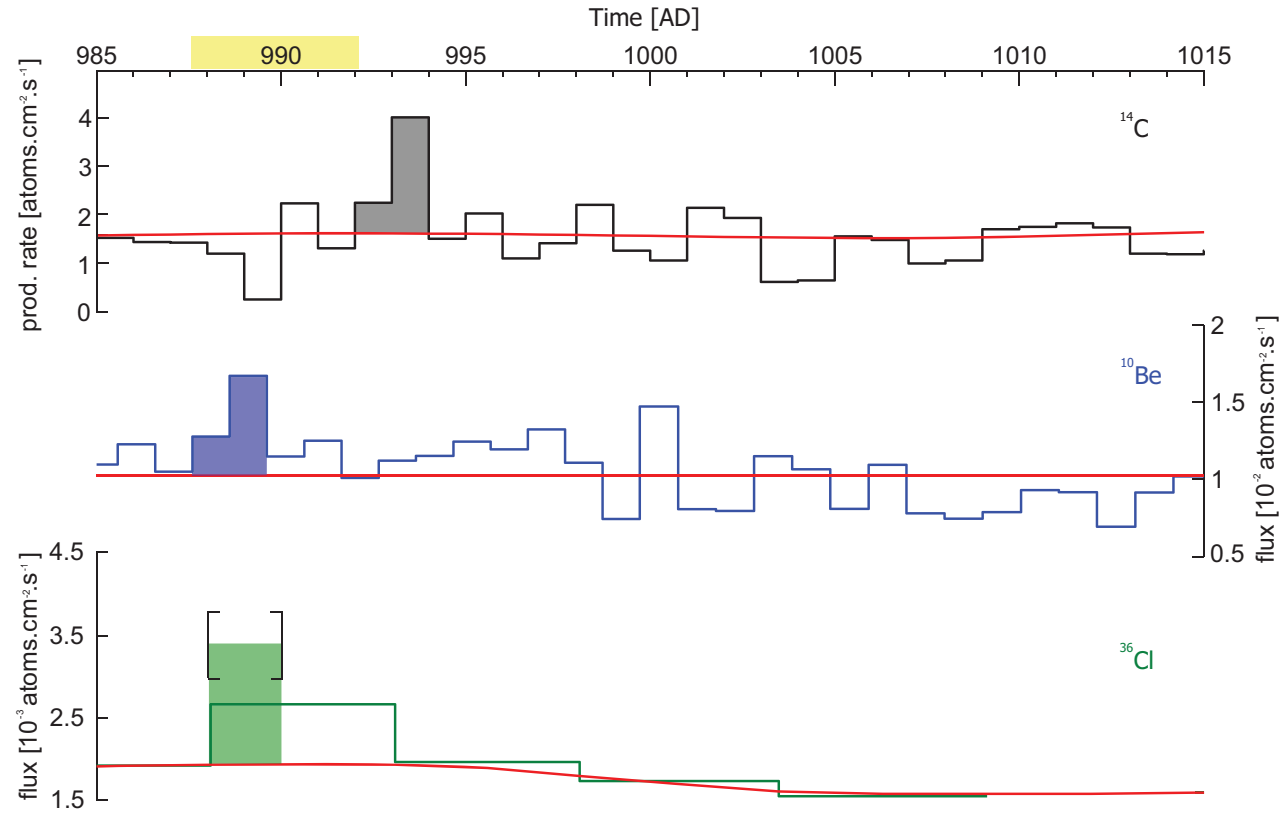

Fig. 11b. Surplus of radionuclides production and flux induced by the M13 event (AD 992/3).

assumes that variations of ^{36}Cl mimics those of ^{10}Be which, based on the NGRIP results, would mean that the remaining 3 years are composed of concentrations in fact 21% higher than the background level. As a result, the production surplus in chlorine-36 is assessed to a factor of 1.55 ± 0.42 during the M13 event.

It is very interesting to note that the M13 event has caused a 30% increase in radionuclides production relative to that of the M12 event. That is with the exception of ^{14}C whose M13 event-related production surplus equals 47% than that of M12. This confirms that the AD 774/5 event was substantially more energetic (Miyake et al., 2013) as it produced substantially more ^{10}Be, ^{14}C and ^{36}Cl.

To summarize (table 4) the M12 event, and to a lower extent the M13 event, yielded considerable enhancements in radionuclide production rates. As a matter of fact, the new ^{10}Be measurements indicate an increase of 325% for the M12 event which is in agreement with ^{14}C. As for ^{36}Cl, it exhibits the largest increases with production excess of about 512% and 155% for the M12 and M13 events, respectively.

4.2 Glaciochemical data during the events

4.2.1 δ^{18}O records

Principal component analysis (PCA) was applied on the common time period of the four ice cores spanning through a total of 1,320 years ie. AD 553-1872. The eigenvalues of Dye 3, Crete, GRIP and NGRIP on the different principal components are given in table 5. The table furthermore shows that each ice core contributes with the same sign to the first principal component (PC1) which confirms the regional aspect of the derived signal as plotted in fig. 12 (Vinther et al., 2003). The explained variance of PC1 is equal to 41.26%. In other terms, nearly half of the δ^{18}O variance in the four ice cores is regionally represented. PCA was also carried out on four noise series sharing the same spectral characteristics as the four δ^{18}O records used with a PC1 explained variance found to only reach 27.64%. This advocates for PC1 to not only being composed of noise (Vinther et al., 2003).

Figure 12 depicts the derived PC1 in addition to the four δ^{18}O records during AD 700-1100. It allows one to visually assess that both events are not associated with any particularly outstanding excursion in δ^{18}O. Although, it should be mentioned that the AD 774/5 event (AD 767-9 as seen in ice cores from Greenland) does correspond with an increase in PC1 δ^{18}O exceeding the standard deviation of 1.35. This is nevertheless not a significant result given that the record encompasses 205 such positive excursions which accounts for 15.5% of PC1 time series. One can also observe that a noticeable depletion in δ^{18}O reaching 1.7σ occurs in Dye 3 ice core during the M12 event. This, in contrast, is more significant as only 5.98% of the whole 1,320 years record features at least as low δ^{18}O values. None of the three other ice cores show visually striking characteristics during neither the M12 nor the M13 events.

While there are *a priori* no proportional responses of δ^{18}O to the cosmogenic radionuclides spikes, this does not necessarily preclude that both events had an impact on air temperature and/or on the transport and fractionation of oxygen isotopes. As such, Pearson correlations between ^{10}Be from NGRIP and δ^{18}O from the four ice cores as well as the derived PC1 are displayed with associated significances in table 6 . In accordance with what can be visually

Table 4. Parameters of both the M12 (AD 774/5) and the M13 events (AD 992/3) as recorded in multiple radionuclide records and as seen in fig. 11.

	^{14}C prod. rate *(cm^{-2}s^{-1})*	^{10}Be flux *(cm^{-2}s^{-1})*	^{36}Cl flux *(cm^{-2}s^{-1})*
M12 event:			
Background level	1.54	0.0091	0.0017
Production surplus	6.13	0.0297	0.0086±0.003
Surplus factor:	3.98	3.25	5.12 ± 1.75
M13:			
Background level	1.63	0.0102	0.0018
Production surplus	3.04	0.009	0.0028±0.0007
Surplus factor:	1.87	0.88	1.55 ± 0.42

Table 5. Principal Components weights of the 4 ice cores in addition to the explained variance of each components. Dye 3 represents Southern Greenland, Crete and NGRIP represent Central Greenland while NGRIP represents Northen Greenland.

	PC1	PC2	PC3	PC4
Dye 3	0.1681	-0.2084	0.9470	0.8457
Crete	0.4210	-0.3278	0.0116	0.8457
GRIP	0.7233	-0.3690	-0.3030	-0.4989
NGRIP	0.52 10	0.8444	0.1058	0.0664
Variance	41.26%	23.79%	18.18%	16.77%

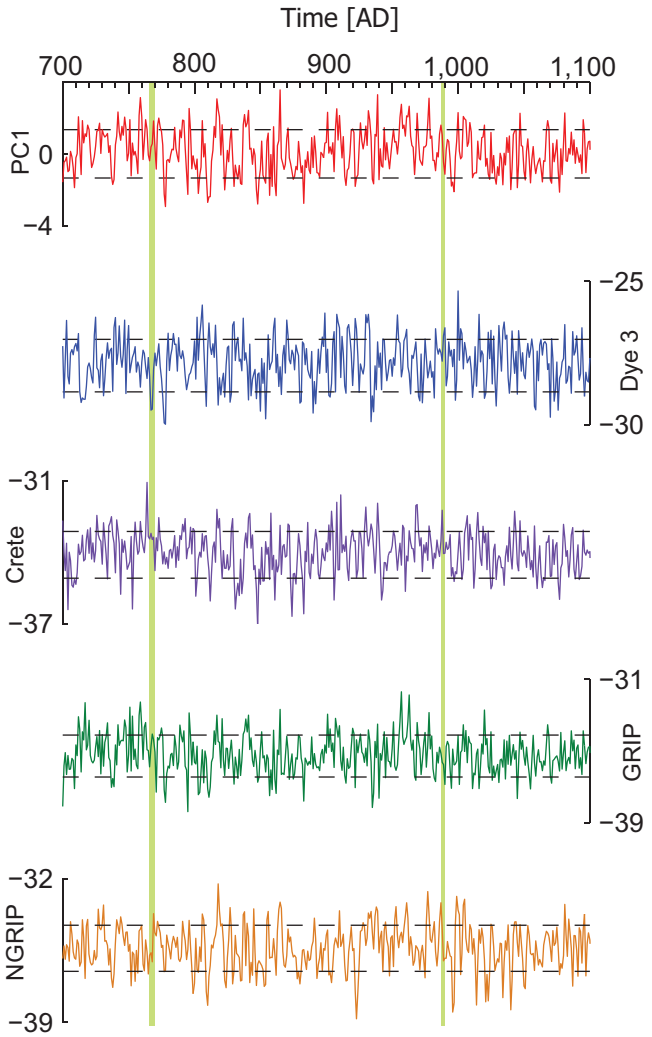

Fig. 12. PC1 and related $\delta^{18}O$ time series. Dashed lines represent standard deviations (+/-) ie. the gap between both lines represent 2σ. Green shaded area represents the time period corresponding to the M12 and the M13 events considering the GICC05 time scale offset.

established from fig. 12, only Dye 3 exhibits interesting relations to M12 at AD 767-69. Indeed, Dye 3 $\delta^{18}O$ is nearly half anti-correlated to NGRIP ^{10}Be with 98% significance (ie. $p<0.02$). Pedro et al. (2006) proposed that an anticorrelation exists between ^{10}Be and $\delta^{18}O$. Indeed, these authors argue that ^{10}Be can be scavenged by warm air masses with water vapor enriched in ^{18}O as opposed to colder air masses with water vapor depleted in ^{18}O. This leads to a potential for confounding solar modulation with climatic modulation (Pedro et al., 2006). In order to untangle this link, correlation coefficients were also calculated for the same time period but excluding the ^{10}Be spike. The value of only -0.22 shows that the event is still potentially largely responsible for the half anti-correlation.

Interestingly, GRIP and NGRIP $\delta^{18}O$ portray positive correlations to NGRIP ^{10}Be, albeit this is of

Table 6. Pearson correlations to NGRIP ^{10}Be of the four ice cores $\delta^{18}O$ for both the M12 and M13 events (time frames are AD 765-792 and AD 985-1015). p-values calculated with Montecarlo simulations show the significance of the relevant r^2 values. Correlations with the ^{10}Be peaks removed are also present. Numbers in the brackets mean that a lag of such years had to be accounted for in order to yield better correlations.

	Dye 3	Crete	GRIP	NGRIP	PC1
M12 event:					
r^2 *(lag yrs)*	-0.48	0.03	0.22	0.23 *(1)*	0.09
p *(lag yrs)*	<0.02	-	<0.16	<0.17 *(1)*	-
r^2 *(w/o peak)*	-0.22	-	-	-	-
M13 event:					
r^2 *(lag yrs)*	0.35	-0.09	-0.4 *(1)*	-0.24	-0.25 *(1)*
p *(lag yrs)*	<0.03	-	<0.02	<0.13	<0.13
r^2 *(w/o peak)*	0.35	-	-0.29	-	-

low importance considering the poor significance. The fact that Dye 3 exhibits such different results and behavior is not surprising and is expressed by its little weight on the first principal component (table 5). This can be explained by the location of Dye 3, as depicted in fig. 5, which is the southernmost as well as closest to the sea and most separated ice core of the four.

Even though the correlation between Dye 3 $\delta^{18}O$ and NGRIP ^{10}Be is well significant, it is possible that high frequency cycles forced by climate oscillations such as the North Atlantic Oscillation (NAO) or forced by solar activity would occur. This would likely to not be expressed in the red noise series used to test the correlation significances. To investigate this possibility and with concern for robustness, a continuous wavelet transform (CWT) for the time period AD 700-900 was applied to the Dye 3 $\delta^{18}O$ signal and is shown in fig. 14. The wavelet analysis (Grinsted et al., 2004) emphasizes that significant ~11-years and a ~22-26-years cycle occur stochastically throughout the record. As a matter of fact, the drop in $\delta^{18}O$ associated with M12 proves to be timed with the onset of such an 11-years cycle. This phenomenon casts doubts on the role of the event on $\delta^{18}O$ variance in Dye 3 at AD 767-69 as it is likely to be induced by a normal climate oscillation. Intriguingly, the negative excursions in $\delta^{18}O$ related to the 11-years cycle in the CWT during the period AD 760-785 matches well the solar modulation inferred by the NGRIP ^{10}Be data (fig. 11a).

As for the M13 event, Dye 3 shows contrarily a positive correlation to NGRIP ^{10}Be albeit all of it can be explained without the peak (table 4). A significant correlation also exists between NGRIP $\delta^{18}O$ and ^{10}Be given a 1 year lag. Nevertheless, most of it can also be

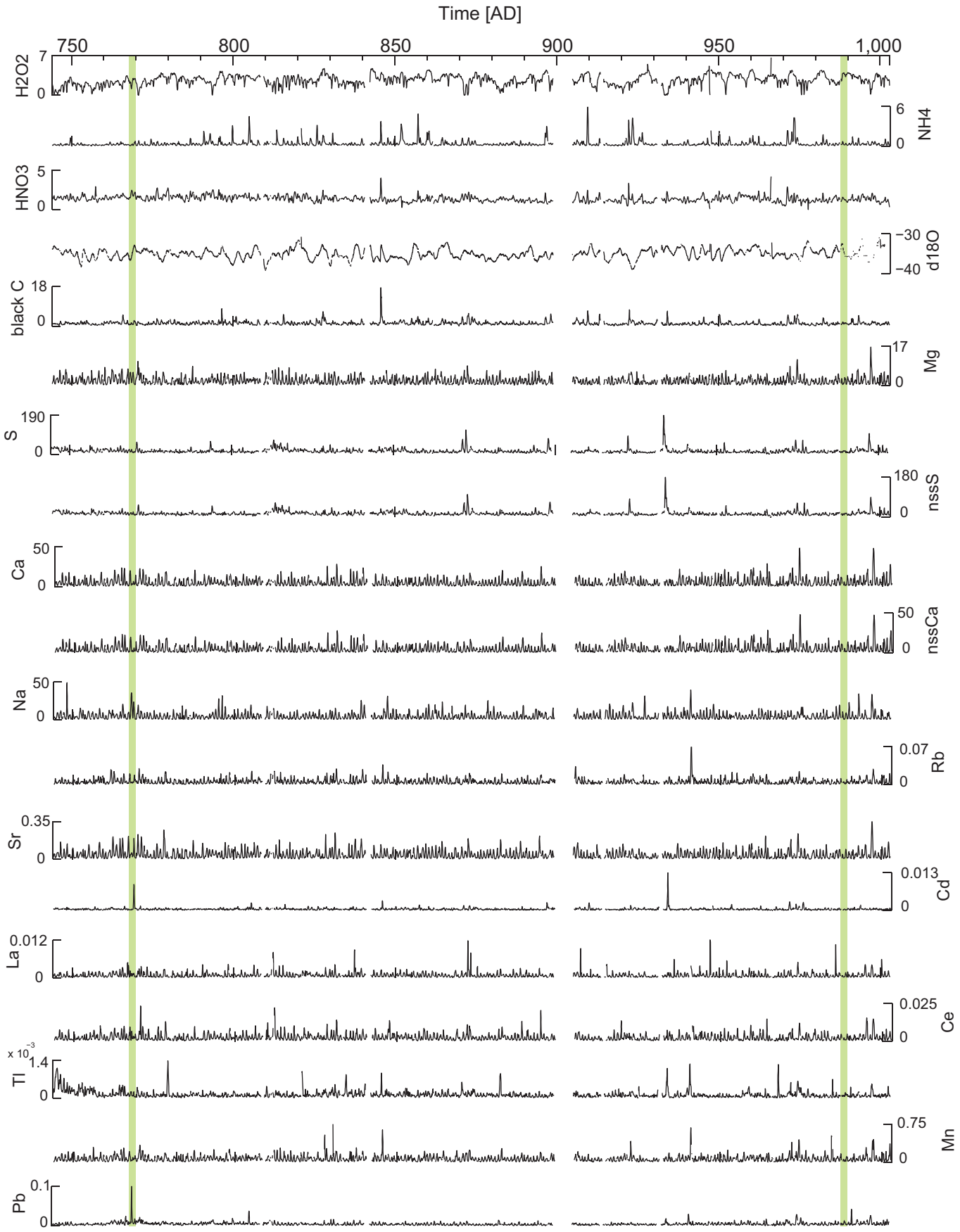

Fig. 13. Continuous flow analysis (CFA) time series from NGRIP for AD 744-1003. The values are in ppb apart from H_2O_2, NH_4 and HNO_3 which are in µM. The green shadings emphasize the time periods of occurence of the M12 and M13 events.

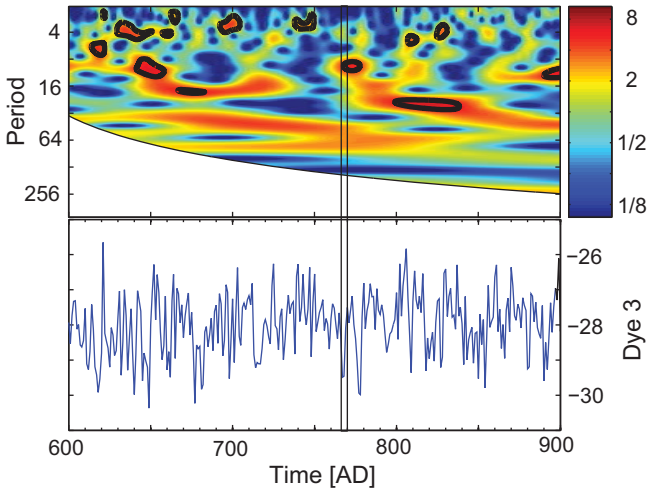

Fig. 14. Upper panel: Continuous wavelet transform (CWT) for $\delta^{18}O$ from NGRIP. Periods represent cycle lengths, the color scale represents the spectral power. Contour lines represent significant ($p<0.05$) results. The edged out area corresponds to the cone of influence (Grinsted et al., 2004). Wavelet analysis is described in §3.3.6. Lower panel: the Dye 3 $\delta^{18}O$ time series. The framed period correspond to the M12 event..

explained without the ^{10}Be peak. Both correlation coefficients are consequently regarded as irrelevant in regards of a potential effect of the M13 event.

In sum, despite interesting correlations there does not seem to be any relevant and significant link between $\delta^{18}O$ in Greenland ice cores and both the M12 and M13 events.

4.2.2 CFA data

In addition, continuous flow analysis (CFA) data from NGRIP was used. The fact that both these data and ^{10}Be come from the same archive allows for excellent time control. The raw dataset is presented in fig. 13. At first glance, one can see that sporadic outliers are present at AD 768 such as sodium, lead and cadmium and at AD 770 such as magnesium and sulfur. The most striking feature of the figure certainly is the spike in lead which is out of proportion during the M12 event and to a lesser extent the one in cadmium. It is also interesting to note that most impurities have a strong seasonal signal which renders many yearly oscillations with the timing of peaks and troughs differing from elements to elements.

It is evident that many microparticles have similar bulk behavior and thus record the same forcing. Owing to this, PCA was used on annually averaged concentrations. The analysis was carried out on the whole period covered by the data ie. AD 744-1,003 and only elements and ions were used, excluding chemical compounds. Figure 15 shows the 4 first eigenvectors from the PCA plotted against each other which allow for visually extracting patterns in groupings of the elements (Boutron & Martin, 1980). As such, 4 groups of highly inter-correlated elements are derived with group 1 composed of all the trace elements: Mn, Rb, Sr, Cd, La, Ce, Tl and Pb; group 2 composed of: both S and nssS; group 3 composed of both Ca and nssCa in addition to Mg; and finally group 4 composed of only Na.

The clear clustering in elements strongly suggests that several air masses of different sources are responsible for the variance seen in the CFA data (fig. 14). Indeed, it has already been established that trace elements (group 1) as archived in ice cores originate from crustal and/or anthropogenic sources (Candelone et al., 1995; Boutron et al., 1995). Volcanic eruptions can also release important amounts of such elements in the atmosphere (Herron et al., 1977; Matsumoto & Hinkley, 2001). As for group 2, background levels of sulfate are usually associated with biogenic production while volcanic eruptions often cause sporadic outliers (Mayewski et al., 1993). Group 3 and 4 are characteristically interconnected throughout the record and are well correlated though elements constituting group 3 are associated with continental dust while Na is a known sea spray marker (Twickler & Whitlow, 1995).

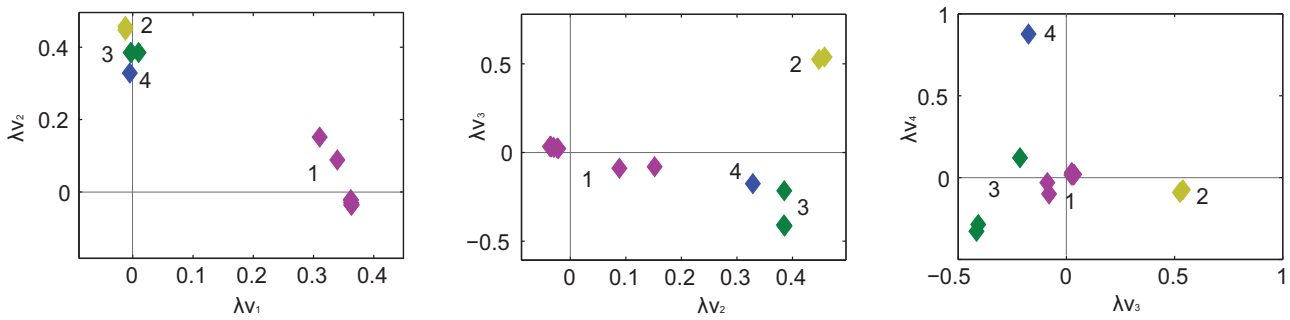

Fig. 15. First four eigenvectors (λv_1, λv_2, λv_3 and λv_4) plotted against each other. Four clustering pattern emerges. Group 1 (in purple) is composed of all trace elements; group 2 (in yellow) is composed of S and nssS; group 3 (in green) is composed of Ca, nssCa and Mg; group 4 (in blue) is composed of Na. The eigenvectors account for 83, 11.05, 3.97 and 1.70% of the (normalized) explained variance, respectively.

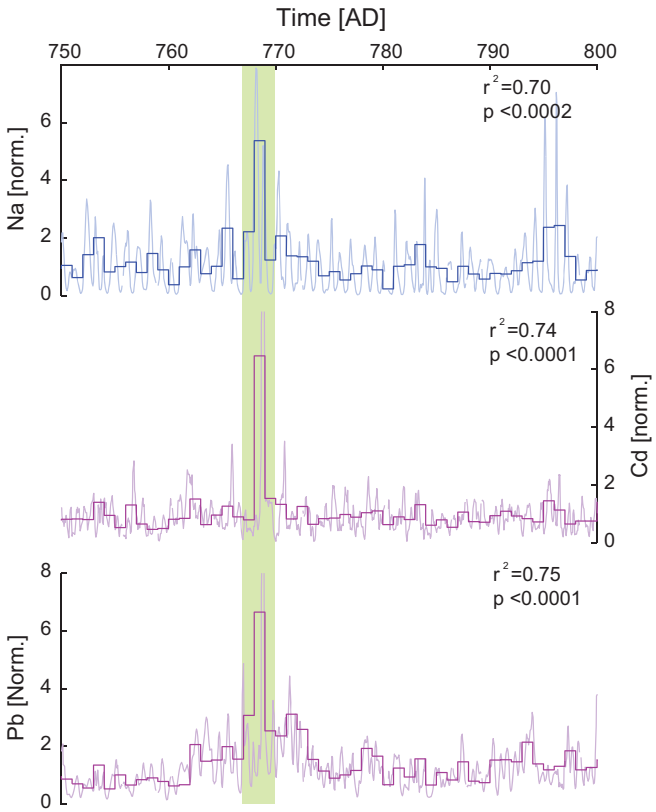

Fig. 16 Sub-annual and annually averaged time series of Na, Cd and Pb during the M12 event. The colors are in relation with the groups from fig. 15. Pearson correlations were calculated between the annually averaged time series of the 3 elements and the NGRIP ^{10}Be data during the period AD 765-792. The green shading emphasizes the time period of occurence of the M12 event.

In sum, the variance of the CFA data is consistent with known sources and can thus be used to infer past changes in atmospheric circulation. There are three elements which feature outliers during the M12 event which are Na, Pb and Cd and are displayed as normalized annually weighted concentrations with correlation coefficients to ^{10}Be in fig. 16. These results demonstrate that sporadic events in Na, Pb and Cd are significantly correlated to ^{10}Be production related to the M12 event. Put more broadly, a sudden strengthening in source and/or transport of marine and anthropogenic and/or continental air masses is recorded in NGRIP at AD 768 and is significantly correlated, both in timing and probability, with the M12 event. However, no noticeable patterns arise from the CFA data during the M13 event.

5 Discussion

5.1 Assessing the causes of the events

The signatures of cosmic-ray increase of AD 774/5 and AD 992/3 have been attributed to many astrophysical sources, some more exotic than others. It should be recalled that while Melott & Thomas (2012) and Usoskin et al. (2013) argued for a solar origin, Hambaryan & Neuhauser (2013) and Pavlov et al. (2013) rather advocated for the events having been caused by a short gamma-ray burst (GRB). More recently, Liu et al (2014) suggested that a comet colliding with Earth's atmosphere could be responsible for the enhanced production seen in ^{14}C. Most of these studies rely on a numerical approach with models of nuclear cross sections such as the *GEANT4* toolkit (Agostinelli et al., 2000) in order to explain the puzzling M12 event. The nuclear cascade leading to radiocarbon production can be triggered by different primary particles (eg. protons and photons) with similar energy levels (fig. 18-19) which may be why the discussion concerning the M12 event, and to a lesser extent the M13 event, still remains an open question. To resolve this issue, a more practical and experimental approach was attempted by using multiple cosmogenic radionuclide records including the new annually resolved NGRIP ^{10}Be measurements from this study. This is considered to provide a better constraint on the causes of the events as shown further in this section. Emphasis will be on the larger of events ie. M12.

5.1.1 A comet?

Liu et al. (2014) reported a large increase in radiocarbon around AD 773 in coral skeletons from the South China Sea which they attribute to a comet which collided with Earth's atmosphere on the 17th of January 773. Indeed, comets are exposed to cosmic radiation and can thus be expected to have higher ^{14}C/^{12}C ratios than Earth's atmosphere (Liu et al., 2014) because of the lack of the geomagnetic field. However, their main argumentation is the timing between the ^{14}C spikes and the cometary event reported in the Old Tang Dynasty Book at AD 773. This approach lacks quantitative and qualitative information of the resulting production excess in ^{14}C. In that light, Usoskin & Kovaltsov (2014) calculated that such a comet would have had to be as large as at least 100 km in diameter to account for the measured radiocarbon increase. As pointed out by the latter authors, this would obviously have had enormous

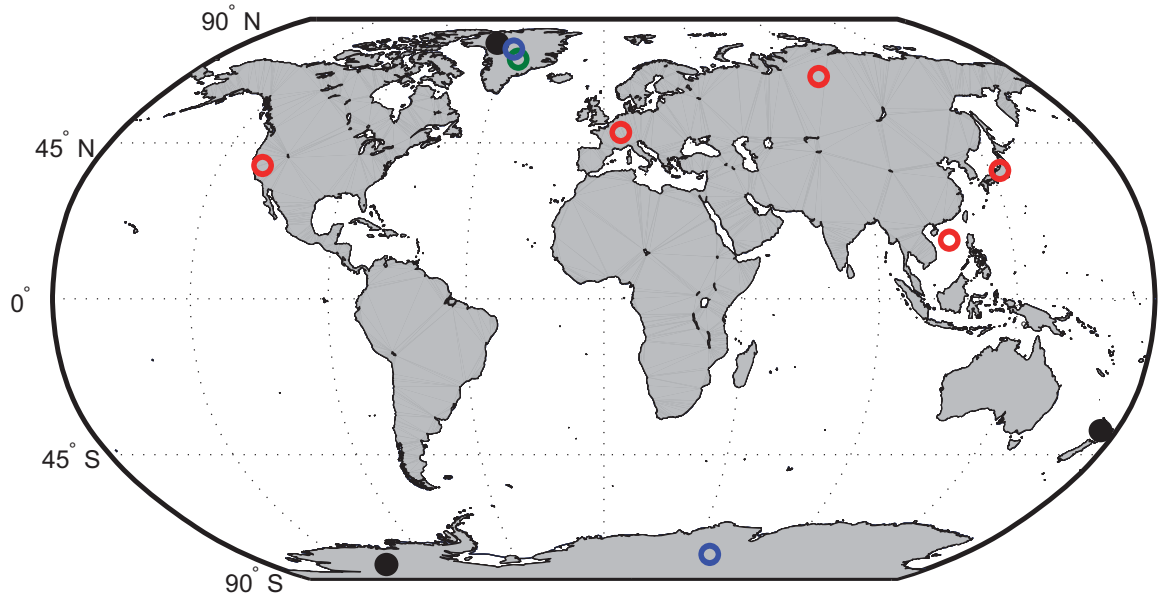

Fig. 17. World map exhibiting in which locations has the M12 event been measured. Red dots are for ^{14}C, blue dots are for ^{10}Be, green dots are for ^{36}Cl and black dots represent unpublished records. Measurements are from: Wagner et al. (2000), Horiuchi et al. (2008), Miyake et al. (2012), Usoskin et al. (2013), Liu et al. (2014), Jull et al. (2014), this study and personal communications.

geological and biological repercussions which could not have gone unnoticed. In addition, dust rain from a comet loaded with radionuclides would have, at most, been localized to only one hemisphere (Jull et al., 2014). However, excursions related to the M12 event have now been reported around the globe in both hemispheres (fig. 17). The comet hypothesis can consequently be discarded.

5.1.2 A supernova?

A supernova origin was one of the early explanations as it could theoretically produce large amounts of ^{14}C and ^{10}Be. For instance, cosmic-rays such as gamma-rays (photons) would generate atmospheric neutrons through photonuclear reactions (Zhou et al., 2013) which in turn would lead to the production of ^{14}C through the reaction $^{14}N(n,p)^{14}C$ (read 1 neutron + 1 ^{14}N atom gives 1 proton + 1 ^{14}C atom). However, Miyake et al. (2012) calculated that the supernova would have had to be as close as < 2 kpc considering typical gamma-ray energies released by supernovae ie. 3 x 10^{51} erg. They also note that a supernova would have resulted in a very bright (in radio and X-rays) remnant which should be readily observable. Even though supernovae could in principle produce substantial amounts of radiocarbon, such a scenario has never been recorded, in particular for SN1006 and SN1054 (Miyake et al., 2012). In accordance, a supernova origin is considered as not responsible for the M12 and M13 events (Miyake et al., 2012; Usoskin et al., 2013; Hambaryan & Neuhauser, 2013, Zhou et al., 2013).

5.1.3 A short gamma-ray burst?

One of the main suggestion for a potential source of the M12 event, and widely relayed by the media, is a short-duration (<2 s) gamma-ray burst which was first proposed by Hambaryan & Neuhauser (2013). Such GRBs emit harder photons than their counterparts with longer duration and most likely result from the merger of compact binary systems such as neutron stars and black holes (Nakar, 2007). Hambaryan & Neuhauser (2013) found that the production of ^{14}C and ^{10}Be as seen in Dome Fuji for the M12 event is consistent with the energetics and the typical spectrum of such short GRBs. In addition, they conjecture that the astrophysical source must have been at least 1-4 kpc far and consequently situated in our galaxy. For comparisons, the center of the Milky Way is more than 8 kpc away from Earth which corresponds to 26,000 light-years. The higher bound of 4 kpc is the maximum distance to yield such an increase in radiocarbon. The lower bound of 1 kpc is explained by the fact that any GRB too close to Earth would have resulted in severe atmospheric ionization leading to ozone depletion of a lethal level. Indeed, a typical GRB can release as much energy in a few seconds than the sun in its entire lifetime (Zhou et al., 2013).

However, Hambaryan & Neuhauser (2013) utilized the ^{14}C production rate as calculated by Miyake et al. (2012) who used an inappropriate carbon

cycle model (Melott & Thomas, 2012). As a result, their ^{14}C production excess (6 x 10^8 atoms.cm^{-2}) is overestimated by a factor of 4.6 as compared to Usoskin et al. (2013; 1.3 x 10^8 atoms.cm^{-2}). When compared to the ^{14}C production surplus of this study (fig. 11a), the overestimation is of a factor of 4 when the one-year spike is considered (1.5 x 10^8 atoms.cm^{-2}) and of 3 when the 3 years-total increase is considered (2 x 10^8 atoms.cm^{-2}). Moreover, they used the ^{10}Be measurements from the Dome Fuji ice core which has unsuitable resolution. Hambaryan & Neuhauser (2013) also mistakenly used the mean resolution of the record (10 years) while the resolution at the time period of the event is 15 years.

More recently, Pavlov et al. (2013) also argued for the possibility of a short-hard GRB as the source of the M12 event using a revised ^{14}C production rate. Their approach was to predict the production of different radionuclides by modeling the photonuclear reactions of primary gamma-rays with atmospheric atoms using yield functions by photons as depicted in fig. 18. By doing so, they show that high energy gamma-rays (E > 10MeV) do not produce measurable excess of ^{10}Be in the atmosphere. According to the authors, this is due to the fact that the energy range of the secondary neutrons is below the ^{10}Be spallation threshold ie. E < 20 MeV. Another feature of the production of radionuclides induced by short-hard GRBs is that secondary neutrons of an energy of ~1 MeV can produce chlorine-36 through the $^{36}Ar(n,p)$ ^{36}Cl channel reaction whose threshold is at ~0.5 MeV. This typical feature constitute the 'isotopic footprint' of GRBs (Pavlov et al., 2013) with considerable production of ^{36}Cl and ^{14}C and none of ^{10}Be. Nevertheless, the authors point out that GRB-induced radiation must produce strong ionization in the atmosphere which would yield large amounts of NO_x in the stratosphere and which are a catalyst of ozone depletion. They then conjecture that such ozone depletion would lead to a rise of the tropopause facilitating and accelerating stratosphere-troposphere exchanges. This would thus lead, still according to Pavlov et al. (2013), to a sustained injection of stratospheric air into the troposphere resulting in an additional supply of radionuclides. Beryllium-10 deposition rate could consequently rise despite the production remaining constant. They further conjecture that the Arctic would be less prone to this phenomenon which would result in a bi-polar asymmetry in ^{10}Be ice concentrations. Put more simply, Pavlov et al. (2013) show that a typical short GRB signature on radionuclide records would be a measurable excess of ^{14}C and ^{36}Cl and of potentially Antarctic ^{10}Be.

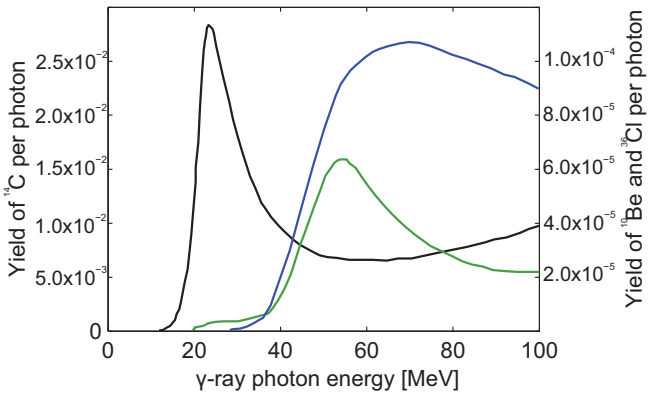

Fig. 18. Yield functions for ^{14}C (black), ^{10}Be (blue) and ^{36}Cl (green) by γ-rays. Modified from Pavlov et al., 2013.

However, the new NGRIP ice core measurements from this study clearly exhibit a large production excess in ^{10}Be (fig. 11a) similar to that of radiocarbon. This result strongly advocates against the possibility of a short GRB to be the origin of the M12 (and M13) event based on Pavlov et al. (2013) calculations. Furthermore, when averaged to the resolution of Dome Fuji, it is found that the mean production was similar in the Arctic and the Antarctic ie. +22%. This lack of bi-polar asymmetry also speaks against a short GRB. As shown in fig. 17, the M12 event was admittedly global in aspect. With this in mind, it is hard to attribute it to a GRB as they are believed to represent rather narrow beams (Zhou et al., 2013) and that gamma-rays (photons) are undisturbed by magnetic fields. Therefore, it is to be expected that such an event would only affect one hemisphere. A short gamma-ray burst is consequently inconsistent with the NGRIP ^{10}Be measurements, the bi-polar symmetry in ^{10}Be and the global aspect of the event.

5.1.4 A solar proton event?

Based on literature and all available cosmogenic radionuclide records, a comet, a supernova and a short gamma-ray burst have been discredited as a potential source of the M12 (and M13) event. Let us now consider the remaining suggestion – a solar proton event.

Although it is an omnipresent source of cosmic rays, a solar source has been prematurely discarded by Miyake et al. (2012) and Hambaryan & Neuhauser (2013) in consequence of their overestimated ^{14}C production rate. Subsequently, Melott & Thomas (2012) and Usoskin et al. (2013) revisited the energy needed from a solar flare and showed that a remarkably strong, though possible, SPE could have yielded such a radiocarbon spike. Usoskin et al. (2013)

also surveyed historical observations of aurora borealis from oriental and occidental chronicles at low latitudes. They report that sightings hint towards increased levels of solar activity around AD 775 but also AD 765-7 and AD 786 which denotes an 11-years periodicity.

While the global aspect of the event (fig. 17) strongly casts doubts on a short GRB origin, it is very well consistent with a solar flare. Indeed the incident protons, as opposed to photons, would be affected by the geomagnetic field and consequently be redistributed to both magnetic poles where the low cutoff rigidities allow for more protons to reach Earth's atmosphere. Then, the different reactions detailed in §2.2 would lead to the production of the different radionuclides which would be mixed, to some extent, hemispherically by stratospheric winds as well detailed for ^{10}Be by Heikkila et al. (2009). Furthermore, the energy range of solar protons (E ~ 0,1 – 1,000 MeV; Shea & Smart, 1990) is within the threshold of ^{10}Be, ^{14}C and ^{36}Cl production (fig. 19). This is in agreement with the clear measured excess of the three radionuclides. When the yield functions of the production of cosmogenic ^{10}Be, ^{14}C and ^{36}Cl by solar protons are normalized to be compared (fig. 19), one can readily visualize that ^{36}Cl is relatively more affected by such particles. This is again supported by the results from this study which showed that the production excess of chlorine-36 caused by the M12 event was increased by the largest factor (table R1). The increased production of both ^{36}Cl and ^{10}Be is a typical aspect of strong SPEs as computed by Webber et al. (2007) and as opposed to the 'isotopic footprint' (Pavlov et al., 2013) of short GRBs.

In the light of available data, of the newly measured NGRIP ^{10}Be as well as of the global aspect of both events, a solar proton event is the only suggested astrophysical source for the M12 and M13 events which is fully consistent. The fact that there are two events with the same relative production patterns also strongly supports a solar origin in probabilistic terms considering that the other suggested causes are expected to occur more rarely.

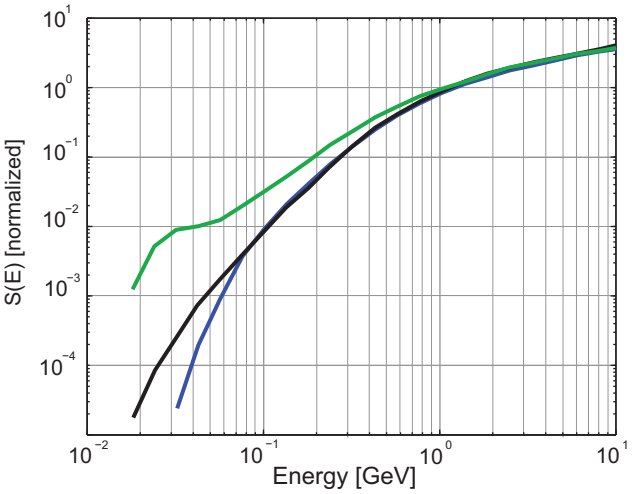

Fig. 19. Normalized yield functions (§3.3.3) for ^{14}C (black), ^{10}Be (blue), ^{36}Cl (green) by protons.

5.2 Parameters of the solar proton events

The fact that a solar flare (M12 event) most likely left such a distinct imprint on ^{10}Be concentration polar ice is puzzling because that would imply that it must have been remarkably strong. Indeed, ^{10}Be has already been tentatively used in order to unravel strong solar proton events passed the instrumental record without yielding much positive results (eg. Usoskin et al., 2006). As a matter of fact, even the biggest historical ground level enhancement (GLE; term explained in §2.5) ever recorded and associated to the SPE of February 1956 did not lead to any substantial excess in ^{10}Be flux. Estimating the parameters and energetics of the associated solar events could consequently be very interesting in regards of our understanding of the solar dynamo.

5.2.1 The energy spectrum

Several studies have attempted to estimate a possible fluence (term explained in §2.5) for the M12 event (Thomas et al., 2013; Usoskin & Kovaltsov, 2012; Usoskin et al., 2013) with results varying as much as 2 orders of magnitude ie. F > 30 MeV (F_{30}) = 3 x 10^{10} to 1.2 x 10^{12} protons.cm^{-2} The discrepancy in estimating the fluence is partly due to the fact that production yields of cosmogenic nuclides, such as radiocarbon, are dependent on the spectrum of a SPE. As such, there are no typical solar events. Therefore, a hard SPE with F_{30} smaller than a very soft SPE may yield the same cosmogenic production. For instance, the computed ^{10}Be and ^{36}Cl productions of historical SPEs from 1940 to 2005 (fig. 20) of Webber et al., (2007) indicate that the SPE of August 1972 (SPE72), which is considered as very soft, produced as much ^{10}Be than the SPE of January 2005 (SPE05) which is considered as hard. However, SPE72 was characterized by a remarkable F_{30} of 4 x 10^9 protons.cm^{-2} – over an order of magnitude stronger than SPE05.

Webber et al. (2007) have listed different F_{30} values and associated relative computed production of ^{10}Be and ^{36}Cl for different historical events. They show by doing so that the hardest recorded SPE (Feb. 1956) with F_{30}=1.8 x 10^9 protons.cm^{-2} yielded 5 times more

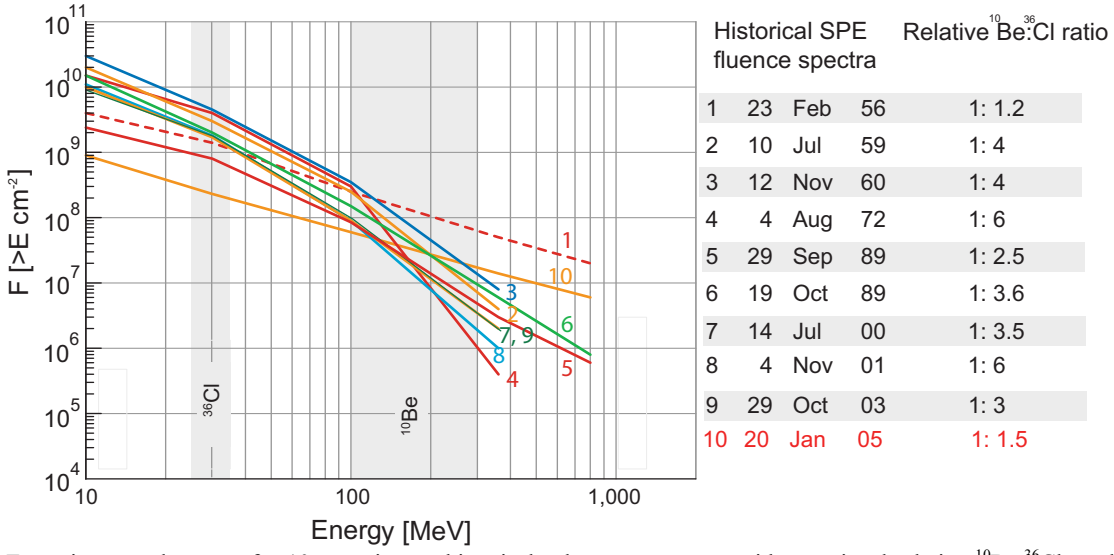

Historical SPE fluence spectra				Relative ^{10}Be:^{36}Cl ratio
1	23 Feb	56		1: 1.2
2	10 Jul	59		1: 4
3	12 Nov	60		1: 4
4	4 Aug	72		1: 6
5	29 Sep	89		1: 2.5
6	19 Oct	89		1: 3.6
7	14 Jul	00		1: 3.5
8	4 Nov	01		1: 6
9	29 Oct	03		1: 3
10	20 Jan	05		1: 1.5

Fig. 20. Event-integrated spectra for 10 conspicuous historical solar proton events with associated relative ^{10}Be:^{36}Cl production ratios. Shaded areas represent the specific peak response energies. Modified from Beer et al. (2012), originally from Webber et al. (2007).

^{10}Be than its softer counterpart (SPE72) which has a a fluence > 30 MeV (F_{30}) twice as large. For ^{36}Cl, the pattern is inverted. This very well exemplifies that radionuclides have fundamentally different peak response energies (Beer et al., 2012). As a result, this discriminant characteristic can be used to our advantage in order to estimate the correct spectrum by comparing the relative ^{10}Be:^{36}Cl ratio of the two events to historical SPEs.

Figure 20 shows different integral spectra of some major instrumental SPEs and associated computed ^{10}Be:^{36}Cl ratios derived from Webber et al., (2007). One can see that the ratios are genuinely different for the different spectra with two groups arising. The hard SPEs (1956, 2005) exhibit ratios lower than 1:2 while the soft SPEs (1959, 1969,1972, 2001, 2003) have ratios typically greater than 1:3 (fig. 20). The relative ^{10}Be:^{36}Cl ratios for the M12 and M13 events are of 1:1.6 (±0.5) and of 1:1.8 (±0.5). Regrettably, the poorly resolved ^{36}Cl measurements do not allow for an accurate estimation of the ratios and thus of the induced spectra. Even so, it can be said that both events relatively produced less than 2.5 times more ^{36}Cl than ^{10}Be, regardless of the different assumptions, which puts both events in the hard spectrum category of solar proton events. The SPE which resulted in the most similar relative ^{10}Be:^{36}Cl ratio is the one from January 2005 with F_{30}= 2 x 10^8 protons.cm^{-2} .

It should be noted that a hard spectrum strengthens the SPE theory because it rules out the inexplicably high and hazardous F_{30} estimates of Thomas et al. (2013) which were based on the very soft SPE of 1972.

5.2.2 The fluence

Having a reliable estimate of the energy spectra in addition to knowing the ^{10}Be flux excess induced by both events, one can theoretically deduce the fluence of the associated SPEs. Webber et al., (2007) computed that the ^{10}Be deposition rate induced by SPE05 was 0.0033 and 0.0005 cm^{-2}s^{-1} assuming no latitudinal mixing and global mixing prior to scavenging respectively. Considering energies of incident protons from SPEs, most production would take place in the stratosphere and thus the latter scenario is the closest to the reality (Beer et al., 2012). With a measured flux of 0.0297 atoms.cm^{-2}.s^{-1}, the ^{10}Be production excess caused by the M12 event is therefore a multiple of 60 of SPE05 (X_{05}=60). As for the M13 event, the measured flux of 0.009 cm^{-2}.s^{-1} gives X_{05}=18. By simply applying the X_{05} multiples to the spectrum of SPE05, it is found that the F_{30} values of the M12 and M13 events are ~1.2 x 10^{10} protons.cm^{-2} and ~3.6 x 10^9 protons.cm^{-2} respectively. Usoskin et al. (2013) utilized a similar technique albeit assuming a spectrum as per SPE56 and using radiocarbon.

It has to be stressed, though, that ^{10}Be fluxes merely represent a deposition rate affected by transport and deposition mechanisms rather than a production rate. As evidenced by fig. 21, the distribution of ^{10}Be deposition flux around the globe is fundamentally bound to precipitation rates so that tropical latitudes will experience the most part of the ^{10}Be deposition and conversely for high latitudes (Heikkilä et al., 2013). This phenomenon was not taken into consideration in Webber et al. (2007) computations. The ^{10}Be-based F_{30} values should therefore be

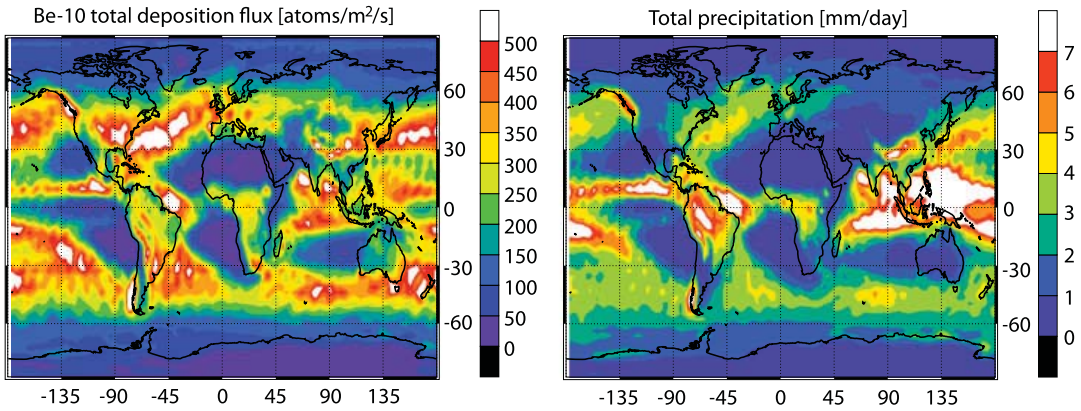

Fig. 21. Deposition flux of ^{10}Be (atoms.m^{-2}s^{-1}), modelled with the ECHAM5-HAM general circulation model, averaged over 1986–1990 (left) and the precipitation rate (mm.day^{-1}). From Heikkilä et al. (2013).

considered as a lower bound or a conservative estimate.

As a check, the modeled ^{14}C production rates were taken in consideration using an alternative technique – response functions (§3.3.3). Using the specific yield function of radiocarbon and the differential energy spectrum of SPE05 (Mewaldt et al., 2005), a multiple X_{05} of 110 and of 52 is needed to explain the production yield of the M12 (2 x 10^8 atoms.cm^{-2}) and M13 (9.4 x 10^7 atoms.cm^{-2}) events respectively. With these multiples, the fluences above 30 MeV (F_{30}) are found to be of 2.2 x 10^{10} protons.cm^{-2} and F_{30} = 10^{10} protons.cm^{-2} for the M12 and M13 SPEs respectively.

5.2.3 Implications

The estimation of possible fluence spectra depicted in fig. 22 involves many assumptions and uncertainties such as the true ^{36}Cl concentration, reliable production rates for ^{10}Be, ^{36}Cl and to a lesser extent ^{14}C and the choice of the spectral fit to name a few. Nevertheless, the following can be said with a good level of confidence. The solar proton event related to the M12 event at AD 774/5 was stronger than any historical solar flare, including the Carrington event. With fluences > 30 MeV of ~1.2 - 2.2 x 10^{10} and ~3.6 - 10 x 10^9 protons.cm^{-2}, the M12 and M13 events were by up to an order of magnitude more energetic than the so far assumed strongest hard SPE (Feb. 1956; fig. 22). Solar proton events most likely need to be characterized by a hard spectrum and to have F_{30} values at least in the vicinity of 10^{10} proton.cm^{-2} in order to leave an imprint on polar ice ^{10}Be concentrations, considering that neither the Carrington event nor the M13 event yielded prominent ^{10}Be spikes. Beryllium-10 is consequently not an ideal detection method for unraveling paleo-solar events. By the same token albeit there is a small enhancement of HNO_3 in the NGRIP CFA data for the M12 event (fig. 13), it is not as conspicuous as one would expect (McCracken et al., 2001; 2004) which confirms doubts on the reliability of nitrate as a SPE marker in ice cores (Wolff et al., 2012). According to the available data, chlorine-36 stands out as the best detection method of past solar proton events owing to its energy peak response of ~30 MeV.

Both inferred SPEs were remarkably strong albeit not that strong that it would have depleted ozone to hazardous levels as it has been suggested (Miyake et al., 2012; Melott & Thomas, 2012; Thomas et al., 2013; Cliver et al., 2014). Furhermore, it should be mentioned that very energetic super flares have been observed in solar-type stars (Nogami et al., 2014) which further strengthens the SPE hypothesis.

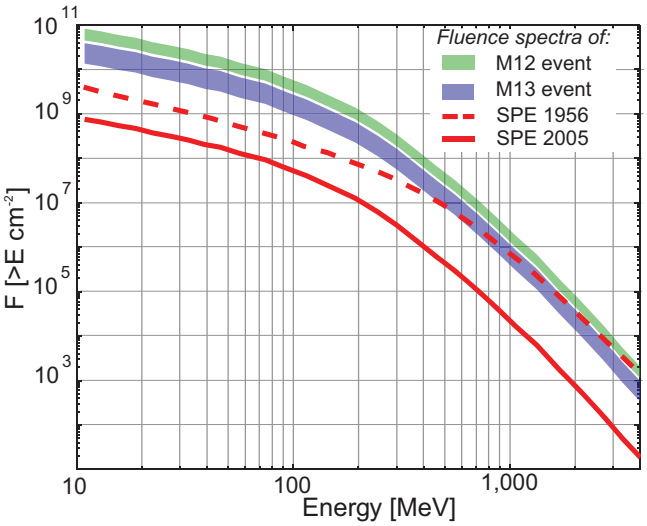

Fig. 22. Possible event-integrated fluence spectra for the M12 (green shading) and M13 (blue shading) events related solar flares. The spectra of SPE56 (dashed red line) and of SPE05 (red line) are also plotted as a reference.

5.3 Potential effects on atmospheric chemistry and circulation

5.3.1 Data interpretation

Three elements are characterized by distinct extremes (fig. 13) in NGRIP ice concentrations coeval with the M12 event which are lead (Pb), cadmium (Cd) and sodium (Na). Lead and cadmium are non-ferrous heavy metals which are usually linked to anthropogenic emissions (Candelone et al., 1995; Boutron et al., 1995) and/or volcanic eruptions (Herron et al., 1977; Matsumoto & Hinkley, 2001). In this case, it is unlikely that a volcanic eruption is responsible for the sporadic increase in Pb and Cd because of the lack of a sulfur (S) spike in the CFA time series (fig. 13). Indeed, individual peaks in ice core sulfates are commonly used as a tracer of explosive eruptions (Matsumoto & Hinkley, 2001). A possible example of volcanic-induced enrichment in heavy metals is evidenced at AD 933 (fig. 13) where a S-spike is markedly timed with an annual enhancement of Cd and Ti. Atmospheric pollution therefore stands out as a more likely cause to explain the sporadic Pb and Cd spikes which would not be unheard of for the pre-industrial era (Martinez-Cortizas et al., 2002; Kylander et al., 2005). However the timing, the magnitude and the statistically significant correlation of the two heavy metals to 10Be suggest a link with the exceptional solar proton event. As far as investigated, there are no mentions of such a linkage in the literature and both heavy metals are not considered as indicative of climate variability so that discussing causality is somewhat conjecture. A possible scenario would be that the SPE induced changes in atmospheric circulation patterns leading to more air masses enriched in Cd and Pb to come across northern-central Greenland. The source of such air masses could potentially be isotopically identified and therefore give insights into the possible atmospheric circulation shift that happened at the time period of the M12 event. Such a technique has allowed Rosman et al. (1997) to link a depression in the 206Pb/207Pb ratio to intensive mining in southern Spain some 2,000 years ago. Of course, a coincidental timing between atmospheric pollution and the M12 SPE cannot be excluded.

As for the sodium spike, it shows a strengthening of marine air masses (Twickler & Whitlow, 1995) which would indicate more prevalent storminess and by extension more vigorous atmospheric circulation. As a matter of fact, Dawson

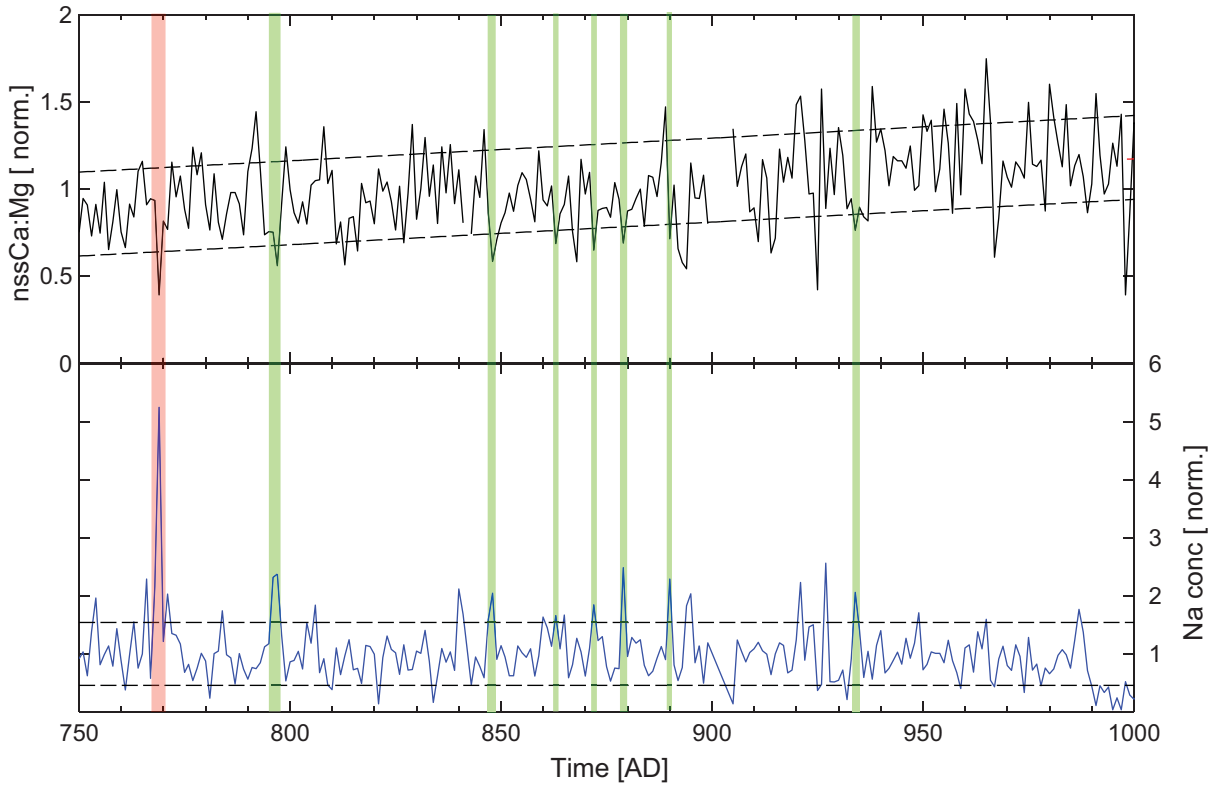

Fig. 23. Computed nssCa:Mg ratio and measured Na conentration (annually averaged) time series from the NGRIP ice core show a recurring, although not ubiquitous, pattern of low extremes of Ca:Mg coeval with high extremes of Na. Dashed lines represent the strandard deviation. Red shading represents the M12 event while green shadings represent other time periods with similar patterns.

et al. (2003; 2007) linked high Na extremes in ice cores from Greenland to instrumental records and historical information of storminess. In addition, Meeker & Mayewski (2002) found that Na from the GISP2 ice core in central Greenland is partly correlated to the Icelandic low which is a component of the definition of the North Atlantic Oscillation (NAO), together with the Azores high. These results tend to suggest that an increase in sea-level pressure gradient in the North Atlantic (NAO+) associated with increased storminess is synchronous with, and possibly caused by, the solar proton event related to the M12 event.

Interestingly, the nssCa:Mg ratio as plotted in fig. 23 also exhibits a striking (negative) outlier at AD 768 (GICC05 timescale). Data on Ca and Mg dust sources is limited (Twickler & Whitlow, 1995) which renders the interpretation complicated. Nevertheless, it is worth mentioning that a reccuring, although not ubiquitous, pattern arise between negative extremes (-1σ) in Ca:Mg and positive extremes (+1σ) in Na. Indeed, fig. 23 shows that about half of the Na excursions are corresponding to lows in the Ca:Mg ratio. This consistency argues for the Na and Ca:Mg extremes occurring during the M12 event to mirror a particular atmospheric circulation change over northern-central Greenland, most likely linked to increased storminess. It can be argued that the decrease in the Ca:Mg could be explained by the fact that the Mg data encompasses both sea salt and non-sea salt components. As a result, more vigorous marine air masses would automatically reduce the ratio, although the Mg time series (fig. 13) does not exhibit any striking excursions. Alternatively, the low Ca:Mg values could indicate a different dust source.

The CFA data consequently shows that increased marine air masses vigor associated with sustained storminess (Dawson et al., 2003: 2007) and a deepening of the Icelandic low (Meeker & Mayewski, 2002) as well as increased air masses of enriched non-volcanic Pb and Cd are synchronous with the M12 solar proton event. However, it has to be recalled that correlation does not mean causality so that a coincidental timing between the CFA spikes and the M12 event cannot be excluded.

5.3.2 Possible mechanisms

The mechanisms involving solar forcing on climate are considered as very poorly understood. Nevertheless, a number of studies have demonstrated that SPEs largely impact and control ozone levels in Polar Regions. For instance, Lopez-Puertas et al. (2005) investigated the SPEs of October-November and reported arctic enhancements of nitric oxides (NOx) and hydrogen oxides (HOx) with associated ozone (O3) depletion of 30-40% in the upper stratosphere. In addition, they noted unusually large auroral activity during the whole subsequent winter. Similarly, Seppälä et al., (2004) found increases of NOx of several hundreds percent and depletion of O3 of tens percent for several months for the same SPE. Jackman et al. (1990) reported stratospheric effects on NOx caused by the soft SPE of August 1972 which lasted for a year. All these studies show unequivocal evidence that solar proton events have a considerable influence on stratospheric chemistry. The question though, is whether this influence extends to the troposphere and how.

In that light, Veretenenko & Thejll (2005; 2007) reported a lowering of pressure levels in the troposphere accompanied with an increase of cyclonic prevalence near the south-east coast of Greenland synchronous with solar proton events. They invoke the advection of cold air and changes in temperature gradient in the region perhaps induced by variations of upper cloudiness induced by solar particles as a cause. Indeed, Veretenenko et al., (2009) claim that temperature gradients in the arctic frontal zone near the south-east coast of Greenland reveal strong ~10 and ~22 year periodicities which they believe to be related to solar activity cycles. According to the authors, the possible chain of reactions involved behind this solar activity-storminess link could be as follows. Incident energetic particles would result in temperature changes perhaps due to radiative forcing of upper cloudiness which would strengthen the temperature contrast in the arctic frontal zone which would in turn affect the intensity of cyclogenesis.

The hypothesis that SPEs can intensify cyclone regeneration, i.e. deepening of existing low pressure systems, agrees well with the Na spike from the CFA data and represents an attractive explanation. Nevertheless, it should be stressed that the involved mechanisms (Veretenenko et al., 2009) are fundamentally speculative and exceed the scope of this study. Furthermore, the lack of indicators of storminess or strengthening of marine air masses during the M13 event somewhat casts doubts on the systematic efficiency of SPEs to increase cyclogenesis.

More recently, Callisto et al., (2013) investigated the influence of a major SPE similar to the Carrington event by means of climate models. The authors reported statistically significant effects on NOx, HOx, O3 depletion, temperature and zonal wind. According to them, their calculations show that a

decrease in polar stratospheric ozone and temperatures would result in acceleration of zonal winds and changes in surface air temperature. As a matter of fact, Callisto et al., (2013) suggest that a warming of up to 7 K could be experienced in Eastern Europe and Russia.

To summarize, three genuinely conspicuous outliers in Na, Pb and Cd ice concentrations are synchronous with an exceptional SPE associated with the M12 event. While little can be inferred from the two heavy metals, Na is well-established as a proxy for marine air masses prevalence and for storminess (Meeker & Mayewski, 2002; Dawson et al., 2003; 2007). A SPE-North Atlantic storminess link has already been invoked by Veretenenko & Thejll (2004; 2005; 2007) which sheds light on the potential of solar energetic particles to influence polar atmospheric chemistry and circulation. This is very interesting because solar forcing on climate is commonly associated with feedback and amplifying mechanisms paced by the varying total solar irradiance. Should the SPE-storminess link be genuine, this could provide an additional aspect to solar forcing especially that strong solar proton events occur majoritarely during the high phase of the 11-yr cycle.

5.4 Early offset in the Greenland Ice Core Chronology 2005 time scale

To end with, it should be mentioned that another genuinely interesting feature of the two events resides in their time of occurrence based on the Greenland Ice Core Chronology 2005 (GICC05). As the results from the annually-resolved NGRIP ^{10}Be measurements show (fig.11a-b), there is an offset between the GICC05 and tree ring time scales with the former lagging the latter by 4 and 7 years for the M13 and M12 events respectively. That is, the cosmic-ray events are recorded in GICC05 at AD 989 instead of AD 993 and at AD 768 instead of AD 775. It has to be stressed that the offset is unequivocal considering that several ^{14}C records from tree rings and ^{10}Be records from ice cores were measured in independent archives and yielded the same results.

Such an early and large offset is unexpected and startling because the maximum counting error at that time period is considered to be of only 1 year (Vinther et al., 2006). The chronology of the last 2,000 years is based on detailed δ^{18}O data, ions chromatography and electric conductivity measurements (Vinther et al., 2006) with several volcanic eruptions used as tie-points between the different ice cores. Obviously, there are unforeseen issues when dealing with such data which are otherwise expected to exhibit rather clear seasonal and annual cycles. In that light, an effort is currently under way in order to solve this early offset using a new and promising automated layer detection algorithm (Winstrup et al., 2012).

In consequence, the two events shed light on the potential of cosmogenic radionuclides to be utilized as a geochronological tool. Indeed, not only can they be used to compare and synchronize different long-term time scales (eg. Muscheler et al., 2014) but short-term cosmic ray events could also be used as additional tie-points between different ice cores or archives. Such signatures of rapid increase of cosmic-rays, and thus radionuclide production rates, present the advantage of yielding a global signal and of being more straight-forward in terms of interpretation as opposed to volcanic eruptions. Indeed, Coulter et al. (2012) showed that volcanic products in Greenland resulting in the acid signals vary both in space and in time. Cosmic-ray events thus represent valuable and additional isochrones for synchronizing Greenland ice cores but also for synchronizing records from Greenland and Antarctica. The latter fact is genuinely important considering that this would allow better investigations of the bipolar seesaw. More generally, the common signal of cosmic ray flux around the world provides the opportunity to synchronize different archives (Muscheler et al., 2014) such as sediments with ^{14}C and ^{10}Be, speleothems with ^{14}C, corals with ^{14}C and ice cores with ^{10}Be and ^{36}Cl. Cosmogenic radionuclides are thus of great interest for investigating spatial leads and lags in past climate changes.

6 Conclusions

- New annually-resolved ^{10}Be measurements from the NGRIP ice core confirm the global and extremely energetic aspect of the AD 774/5 and AD 992/3 cosmic-ray events with increases of 325% and 88% respectively.
- The new ^{10}Be measurements also shed light on an unexpectedly early offset in the GICC05 time scale with a lag of 4 years at AD 993 (1,007 years b2k) and of 7 years at AD 775 (1,225 years b2k).
- The cosmogenic radionuclide records show full consistency with solar proton events as the cause for the AD 774/5 and AD 992/3 events.

- In the same way, the global aspect of the events in addition to the conspicuous ^{10}Be peaks are in disagreement with short gamma-ray bursts as an origin.
- Using relative ^{10}Be:^{36}Cl ratios, it is found that the two solar proton events had a very hard energy spectrum similar to that of the SPE of January 2005.
- The estimated fluences (>30 MeV) for the SPEs of AD 774/5 and AD 992/3 are of ~1.2-2.2 x 10^{10} protons.cm^{-2} and of ~3.6-10 x 10^{9} protons.cm^{-2} respectively.
- The largest of the two SPEs (AD 774/5) is therefore characterized by a fluence (>30 MeV) an order of magnitude higher than the strongest instrumental hard SPE of February 1956.
- The estimated fluence in addition to the ^{10}Be spike shows that the SPE of AD 774/5 was substantially stronger than the Carrington event of 1859 which is considered as the strongest reported historical solar flare.
- Peaks in Na, Pb and Cd concentrations in the NGRIP ice core provide evidence for atmospheric circulation responses synchronous with the SPE of AD 774/5.
- The increase in Na is interpreted as an increased vigor in marine air masses associated with increased storminess in the North Atlantic coeval with the SPE of AD 774/5. This is in agreement with a suggestion that solar proton events may induce a regeneration of cyclones in this region.

7 Acknowledgements

First and foremost, I would like to thank my supervisor Raimund Muscheler for giving me the opportunity to work on such an exciting and stimulating project, for providing with the modeled ^{14}C production rates, for reviewing the manuscript and for always taking the time to discuss issues and ideas. My co-supervisor Florian Adolphi is also thanked for his insights, helpful Matlab functions and for helping with the sampling of the NGRIP ice. I would like to acknowledge Ala Aldahan, Ann-Marie Berggren and Anna Sturevik Storm from Uppsala University, Sweden for letting me use their ^{10}Be laboratory and for instructing me on how to do the chemical preparation as well as Göran Possnert for the AMS measurements. Also, Anders Svensson from the Centre of Ice and Climate in Copenhagen, Denmark is thanked for allowing us to sample NGRIP ice and Joseph McConnell from the Desert Research Institute in Reno, USA is thanked for sharing his very interesting CFA data. Last but certainly not least, a warm and special thank you goes to my parents for always supporting me and encouraging me – *merci beaucoup*.

8 References

Agostinelli, S., Allison, J., Amako, K. E., Apostolakis, J., Araujo, H., Arce, P., Asai, M., Axen, D., Banerjee, S. & Barrand, G., 2003: GEANT4—a simulation toolkit. *Nuclear instruments and methods in physics research section A: Accelerators, Spectrometers, Detectors and Associated Equipment 506***,** 250-303.

Bard, E., Raisbeck, G. M., Yiou, F. & Jouzel, J., 1997: Solar modulation of cosmogenic nuclide production over the last millennium: comparison between 14C and 10Be records. *Earth and Planetary Science Letters 150***,** 453 -462.

Beer, J. & Mccracken, K., 2012: Cosmogenic radionuclides: theory and applications in the terrestrial and space environments. *Springer***.**

Berggren, A.-M., 2009: Influence of solar activity and environment on 10Be in recent natural archives.*PhD thesis, Uppsala University.*

Berggren, A. M., Beer, J., Possnert, G., Aldahan, A., Kubik, P., Christl, M., Johnsen, S. J., Abreu, J. & Vinther, B., 2009: A 600-year annual 10Be record from the NGRIP ice core, Greenland. *Geophysical research letters 36*.

Boutron, C. & Martin, S., 1980: Sources of twelve trace metals in Antarctic snows determined by principal component analysis. *Journal of Geophysical Research: Oceans (1978–2012) 85***,** 5631-5638.

Boutron, C. F., Candelone, J.-P. & Hong, S., 1995: Greenland snow and ice cores: unique archives of large-scale pollution of the troposphere of the Northern Hemisphere by lead and other heavy metals. *Science of the total environment 160***,** 233-241.

Calisto, M., Usoskin, I. & Rozanov, E., 2013: Influence of a Carrington-like event on the atmospheric chemistry, temperature and

dynamics: revised. *Environmental Research Letters 8*, 045010.

Candelone, J. P., Hong, S., Pellone, C. & Boutron, C. F., 1995: Post-Industrial Revolution changes in large-scale atmospheric pollution of the northern hemisphere by heavy metals as documented in central Greenland snow and ice. *Journal of Geophysical Research: Atmospheres (1984–2012) 100*, 16605-16616.

Castagnoli, G. & Lal, D., 1980: Solar modulation effects in terrestrial production of carbon-14. *Radiocarbon 22*, 133-158.

Clausen, H., Gundestrup, N., Johnsen, S., Bindschadler, R. & Zwally, J., 1988: Glaciological investigations in the Crete area, central Greenland: A search for a new deep-drilling site. *Ann. Glaciol 10*, 10-15.

Cliver, E., Tylka, A., Dietrich, W. & Ling, A., 2014: On a solar origin for the cosmogenic nuclide event of 775 AD. *The Astrophysical Journal 781*, 32.

Coulter, S. E., Pilcher, J. R., Plunkett, G., Baillie, M., Hall, V. A., Steffensen, J. P., Vinther, B. M., Clausen, H. B. & Johnsen, S. J., 2012: Holocene tephras highlight complexity of volcanic signals in Greenland ice cores. *Journal of Geophysical Research: Atmospheres (1984–2012) 117*.

Daubechies, I., 1990: The wavelet transform, time-frequency localization and signal analysis. *Information Theory, IEEE Transactions on 36*, 961-1005.

Dawson, A., Hickey, K., Mayewski, P. & Nesje, A., 2007: Greenland (GISP2) ice core and historical indicators of complex North Atlantic climate changes during the fourteenth century. *The Holocene 17*, 427-434.

Dawson, A. G., Elliott, L., Mayewski, P., Lockett, P., Noone, S., Hickey, K., Holt, T., Wadhams, P. & Foster, I., 2003: Late-Holocene North Atlantic climate 'seesaws', storminess changes and Greenland ice sheet (GISP2) palaeoclimates. *The Holocene 13*, 381-392.

Delmas, R., Beer, J., Synal, H. A., Muscheler, R., Petit, J. R. & Pourchet, M., 2004: Bomb-test 36Cl measurements in Vostok snow (Antarctica) and the use of 36Cl as a dating tool for deep ice cores. *Tellus B 56*, 492-498.

Dickinson, R. E., 1975: Solar variability and the lower atmosphere. *Bulletin of the American Meteorological Society 56*, 1240-1248.

Fasso, A., Ferrari, A. & Sala, P., 2001: Electron-photon transport in FLUKA: status. *Advanced Monte Carlo for Radiation Physics, Particle Transport Simulation and Applications*. 159 pp.

Friedlander, M. W., 1989: Cosmic rays. *Harvard University Press*.

Grinsted, A., Moore, J. C. & Jevrejeva, S., 2004: Application of the cross wavelet transform and wavelet coherence to geophysical time series. *Nonlinear processes in geophysics 11*, 561-566.

Hambaryan, V. & Neuhäuser, R., 2013: A Galactic short gamma-ray burst as cause for the 14C peak in AD 774/5. *Monthly Notices of the Royal Astronomical Society 430*, 32-36.

Heikkilä, U., Beer, J. & Feichter, J., 2009: Meridional transport and deposition of atmospheric 10 Be. *Atmospheric Chemistry and Physics 9*, 515-527.

Heikkilä, U. & Smith, A., 2013: Production rate and climate influences on the variability of 10Be deposition simulated by ECHAM5-HAM: Globally, in Greenland, and in Antarctica. *Journal of Geophysical Research: Atmospheres 118*, 2506-2520.

Herron, M. M., Langway Jr, C. C., Weiss, H. V. & Cragin, J. H., 1977: Atmospheric trace metals and sulfate in the Greenland ice sheet. *Geochimica et Cosmochimica Acta 41*, 915-920.

Horiuchi, K., Uchida, T., Sakamoto, Y., Ohta, A., Matsuzaki, H., Shibata, Y. & Motoyama, H., 2008: Ice core record of< sup> 10</sup> Be over the past millennium from Dome Fuji, Antarctica: A new proxy record of past solar activity and a powerful tool for stratigraphic dating. *Quaternary Geochronology 3*, 253-261.

Huggle, D., Blinov, A., Stan-Sion, C., Korschinek, G., Scheffel, C., Massonet, S., Zerle, L., Beer, J., Parrat, Y. & Gaeggeler, H., 1996: Production of cosmogenic 36Cl on atmospheric argon. *Planetary and space science 44*, 147-151.

Jackman, C. H., Deland, M. T., Labow, G. J., Fleming, E. L., Weisenstein, D. K., Ko, M. K. W., Sinnhuber, M., Anderson, J. & Russell, J. M., 2005: The influence of the several very large solar proton events in years 2000–2003 on the neutral middle atmosphere. *Advances in Space Research 35*, 445-450.

Jackman, C. H., Douglass, A. R., Rood, R. B., Mcpeters, R. D. & Meade, P. E., 1990: Effect of solar proton events on the middle atmosphere during the past two solar cycles as computed using a two-dimensional model. *Journal of Geophysical Research: Atmospheres (1984–2012) 95*, 7417-7428.

Jorgensen, T. & Hansen, A., 2000: Comments on" Variation of cosmic ray flux and global cloud coverage-a missing link in solar-climate relationships" by Henrik Svensmark and Eigil Friis-Christensen [Journal of Atmospheric and Solar-Terrestrial Physics 59 (1997) 1225-1232]. *Journal of Atmospheric and Solar Terrestrial Physics 62*, 73-77.

Jull, A., Panyushkina, I. P., Lange, T. E., Kukarskih, V. V., Myglan, V. S., Clark, K. J., Salzer, M. W., Burr, G. S. & Leavitt, S. W., 2014: Excursions in the 14C record at AD 774–775 in tree rings from Russia and America. *Geophysical research letters*.

Kaufmann, P. R., Federer, U., Hutterli, M. A., Bigler, M., SchüPbach, S., Ruth, U., Schmitt, J. & Stocker, T. F., 2008: An improved continuous flow analysis system for high-resolution field measurements on ice cores. *Environmental science & technology 42*, 8044-8050.

Kirkby, J., Curtius, J., Almeida, J., Dunne, E., Duplissy, J., Ehrhart, S., Franchin, A., Gagné, S., Ickes, L. & Kürten, A., 2011: Role of sulphuric acid, ammonia and galactic cosmic rays in atmospheric aerosol nucleation. *Nature 476*, 429-433.

Koyama, K., 1995: ASCA observations of the Galactic center. *Bulletin of the American Astronomical Society*. 1372 pp.

Kristjánsson, J. E., Stjern, C. W., Stordal, F., Fjæraa, A. M., Myhre, G. & Jónasson, K., 2008: Cosmic rays, cloud condensation nuclei and clouds–a reassessment using MODIS data. *Atmospheric Chemistry and Physics 8*, 7373-7387.

Kylander, M. E., Weiss, D. J., Martínez Cortizas, A., Spiro, B., Garcia-Sanchez, R. & Coles, B., 2005: Refining the pre-industrial atmospheric Pb isotope evolution curve in Europe using an 8000 year old peat core from NW Spain. *Earth and Planetary Science Letters 240*, 467-485.

Lal, D. & Peters, B. 1967: Cosmic ray produced radioactivity on the earth. *In Kosmische Strahlung II/Cosmic Rays II*, 551-612. Springer.

Liu, Y., Zhang, Z.-F., Peng, Z.-C., Ling, M.-X., Shen, C.-C., Liu, W.-G., Sun, X.-C., Liu, K.-X. & Sun, W., 2014: Mysterious abrupt carbon-14 increase in coral contributed by a comet. *Scientific reports 4*.

Lopez-Puertas, M., Funke, B., Gil-López, S., Von Clarmann, T., Stiller, G., Höpfner, M., Kellmann, S., Fischer, H. & Jackman, C., 2005: Observation of NOx enhancement and ozone depletion in the Northern and Southern Hemispheres after the October–November 2003 solar proton events. *Journal of geophysical research 110*, A09S43.

Martınez Cortizas, A., Garcıa-Rodeja, E., Pontevedra Pombal, X., Nóvoa Muñoz, J. C., Weiss, D. & Cheburkin, A., 2002: Atmospheric Pb deposition in Spain during the last 4600 years recorded by two ombrotrophic peat bogs and implications for the use of peat as archive. *Science of the total environment 292*, 33-44.

Masarik, J. & Beer, J., 1999: Simulation of particle fluxes and cosmogenic nuclide production in the Earth's atmosphere. *Journal of Geophysical Research: Atmospheres (1984–2012) 104*, 12099-12111.

Matsumoto, A. & Hinkley, T. K., 2001: Trace metal suites in Antarctic pre-industrial ice are consistent with emissions from quiescent degassing of volcanoes worldwide. *Earth and Planetary Science Letters 186*, 33-43.

Mayewski, P. A., Holdsworth, G., Spencer, M. J., Whitlow, S., Twickler, M., Morrison, M. C., Ferland, K. K. & Meeker, L. D., 1993: Ice-core sulfate from three northern hemisphere sites: Source and temperature forcing implications. *Atmospheric Environment. Part A. General Topics 27*, 2915-2919.

McCracken, K., Dreschhoff, G., Smart, D. & Shea, M., 2004: A study of the frequency of occurrence of large-fluence solar proton events and the strength of the interplanetary magnetic field. *Solar Physics 224*, 359-372.

McCracken, K., Dreschhoff, G., Zeller, E., Smart, D. & Shea, M., 2001: Solar cosmic ray events for the period 1561–1994: 1. Identification in polar ice, 1561–1950. *Journal of Geophysical Research: Space Physics (1978–2012) 106*, 21585-21598.

Mchargue, L. R. & Damon, P. E., 1991: The global beryllium 10 cycle. *Reviews of Geophysics 29*, 141-158.

Meeker, L. D. & Mayewski, P. A., 2002: A 1400-year high-resolution record of atmospheric circulation over the North Atlantic and Asia. *The Holocene 12*, 257-266.

Melott, A. L. & Thomas, B. C., 2012: Causes of an AD 774-775 14C increase. *Nature 491*, E1-E2.

Mewaldt, R., Looper, M., Cohen, C., Mason, G., Haggerty, D., Desai, M., Labrador, A., Leske, R. & Mazur, J., 2005: Solar-particle energy spectra during the large events of October-November 2003 and January 2005. *International Cosmic Ray Conference.* 111 pp.

Miyake, F., Masuda, K. & Nakamura, T., 2013: Another rapid event in the carbon-14 content of tree rings. *Nature communications 4*, 1748.

Miyake, F., Nagaya, K., Masuda, K. & Nakamura, T., 2012: A signature of cosmic-ray increase in AD 774-775 from tree rings in Japan. *Nature 486*, 240-242.

Muscheler, R., Adolphi, F. & Svensson, A., 2014: Challenges in 14C dating towards the limit of the method inferred from anchoring a floating tree ring radiocarbon chronology to ice core records around the Laschamp geomagnetic field minimum. *Earth and Planetary Science Letters 394*, 209-215.

Muscheler, R. & Beer, J., 2006: Solar forced dansgaard/oeschger events? *Geophysical research letters 33*.

Muscheler, R., Beer, J., Kubik, P. W. & Synal, H.-A., 2005: Geomagnetic field intensity during the last 60,000 years based on 10Be and 36Cl from the Summit ice cores and 14C. *Quaternary Science Reviews 24*, 1849-1860.

Muscheler, R., Beer, J. & Vonmoos, M., 2004: Causes and timing of the 8200yr BP event inferred from the comparison of the GRIP 10Be and the tree ring Δ 14C record. *Quaternary Science Reviews 23*, 2101-2111.

Muscheler, R., Joos, F., Beer, J., Müller, S. A., Vonmoos, M. & Snowball, I., 2007: Solar activity during the last 1000yr inferred from radionuclide records. *Quaternary Science Reviews 26*, 82-97.

Muscheler, R. A., 2000: *Nachweis von Änderungen im Kohlenstoffkreislauf durch Vergleich der Radionuklide 10Be, 36Cl und 14C*. Eidgenössische Technische Hochschule Zürich.

Nakar, E., 2007: Short-hard gamma-ray bursts. *Physics Reports 442*, 166-236.

Ney, E. P., 1959: Cosmic radiation and the weather. *Nature 183*, 451-452.

Nogami, D., Notsu, Y., Honda, S., Maehara, H., Notsu, S., Shibayama, T. & Shibata, K., 2014: Two Sun-like Superflare Stars Rotating as Slow as the Sun. *arXiv preprint arXiv:1402.3772*.

Pavlov, A., Blinov, A., Konstantinov, A., Ostryakov, V., Vasilyev, G., Vdovina, M. & Volkov, P., 2013: AD 775 pulse of cosmogenic radionuclides production as imprint of a Galactic gamma-ray burst. *Monthly Notices of the Royal Astronomical Society 435*, 2878-2884.

Pedro, J., Van Ommen, T., Curran, M., Morgan, V., Smith, A. & Mcmorrow, A., 2006: Evidence for climate modulation of the 10Be solar activity proxy. *Journal of Geophysical Research: Atmospheres (1984–2012) 111*.

Reimer, P. J., Bard, E., Bayliss, A., Beck, J. W., Blackwell, P. G., Ramsey, C. B., Buck, C. E., Cheng, H., Edwards, R. L. & Friedrich, M., 2013: IntCal13 and Marine13 radiocarbon age calibration curves 0–50,000 years cal BP. *Radiocarbon 55*, 1869-1887.

Rosman, K. J., Chisholm, W., Hong, S., Candelone, J.-P. & Boutron, C. F., 1997: Lead from Carthaginian and Roman Spanish mines isotopically identified in Greenland ice dated from 600 BC to 300 AD. *Environmental science & technology 31*, 3413-3416.

Schawinski, K., Justham, S., Wolf, C., Podsiadlowski, P., Sullivan, M., Steenbrugge, K. C., Bell, T., Röser, H.-J., Walker, E. S. & Astier, P., 2008: Supernova shock breakout from a red supergiant. *Science 321*, 223-226.

Seppälä, A., Verronen, P., Kyrölä, E., Hassinen, S., Backman, L., Hauchecorne, A., Bertaux, J. & Fussen, D., 2004: Solar proton events of October–November 2003: Ozone depletion in the Northern Hemisphere polar winter as seen by GOMOS/Envisat. *Geophysical research letters 31*.

Shea, M. & Smart, D., 1990: A summary of major solar proton events. *Solar Physics 127*, 297-320.

Siegenthaler, U., 1983: Uptake of excess CO2 by an outcrop-diffusion model of the ocean. *Journal*

of Geophysical Research: Oceans (1978–2012) 88, 3599-3608.

Smart, D., Shea, M. & Mccracken, K., 2006: The Carrington event: Possible solar proton intensity–time profile. *Advances in Space Research 38*, 215-225.

Svensmark, H. & Friis-Christensen, E., 1997: Variation of cosmic ray flux and global cloud coverage—a missing link in solar-climate relationships. *Journal of Atmospheric and Solar-Terrestrial Physics 59*, 1225-1232.

Synal, H.-A., Beer, J., Bonani, G., Suter, M. & Wölfli, W., 1990: Atmospheric transport of bomb-produced 36Cl. *Nuclear Instruments and Methods in Physics Research Section B: Beam Interactions with Materials and Atoms 52*, 483-488.

Thomas, B. C., Melott, A. L., Arkenberg, K. R. & Snyder, B. R., 2013: Terrestrial effects of possible astrophysical sources of an AD 774-775 increase in 14C production. *Geophysical research letters 40*, 1237-1240.

Tinsley, B. A., 2000: Influence of solar wind on the global electric circuit, and inferred effects on cloud microphysics, temperature, and dynamics in the troposphere. *Space Science Reviews 94*, 231-258.

Torrence, C. & Compo, G. P., 1998: A practical guide to wavelet analysis. *Bulletin of the American Meteorological Society 79*, 61-78.

Trauth, M. H., Gebbers, R., Marwan, N. & Sillmann, E. 2007. *MATLAB recipes for earth sciences*, Springer.

Twickler, M. & Whitlow, S., 1995: Complexity of Holocene climate as reconstructed from a Greenland ice core. *Science 270*, 22.

Usoskin, I. & Kovaltsov, G., 2014: A comet could not produce the carbon-14 spike in the 8th century. *arXiv preprint arXiv:1401.5945*.

Usoskin, I., Kromer, B., Ludlow, F., Beer, J., Friedrich, M., Kovaltsov, G., Solanki, S. & Wacker, L., 2013: The AD775 cosmic event revisited: the Sun is to blame. *arXiv preprint arXiv:1302.6897*.

Usoskin, I. G. & Kovaltsov, G. A., 2012: Occurrence of extreme solar particle events: assessment from historical proxy data. *The Astrophysical Journal 757*, 92.

Usoskin, I. G. & Kromer, B., 2005: Reconstruction of the 14C production rate from measured relative abundance. *Radiocarbon 47*, 31-37.

Usoskin, I. G., Mursula, K., Solanki, S., Schüssler, M. & Alanko, K., 2003: Reconstruction of solar activity for the last millennium using 10Be data. *arXiv preprint astro-ph/0309556*.

Usoskin, I. G., Solanki, S. K., Kovaltsov, G. A., Beer, J. & Kromer, B., 2006: Solar proton events in cosmogenic isotope data. *Geophysical research letters 33*.

Veretenenko, S., Dergachev, V. & Dmitriyev, P., 2007: Solar activity and cosmic ray variations as a factor of intensity of cyclonic processes at midlatitudes. *Geomagnetism and aeronomy 47*, 375-382.

Veretenenko, S., Dergachev, V. & Dmitriyev, P., 2009: Long-period variations in the characteristics of frontal zones in the north Atlantic and their relation to solar activity and cosmic ray variations. *Bulletin of the Russian Academy of Sciences: Physics 73*, 410-412.

Veretenenko, S. & Thejll, P., 2005: Cyclone regeneration in the North Atlantic intensified by energetic solar proton events. *Advances in Space Research 35*, 470-475.

Vinther, B. M., Clausen, H. B., Johnsen, S. J., Rasmussen, S. O., Andersen, K. K., Buchardt, S. L., Dahl-Jensen, D., Seierstad, I. K., Siggaard-Andersen, M. L. & Steffensen, J. P., 2006: A synchronized dating of three Greenland ice cores throughout the Holocene. *Journal of Geophysical Research: Atmospheres (1984–2012) 111*.

Vinther, B. M., Johnsen, S. J., Andersen, K. K., Clausen, H. B. & Hansen, A. W., 2003: NAO signal recorded in the stable isotopes of Greenland ice cores. *Geophysical research letters 30*.

Voiculescu, M., Usoskin, I. G. & Mursula, K., 2006: Different response of clouds to solar input. *Geophysical research letters 33*.

Vonmoos, M., Beer, J. & Muscheler, R., 2006: Large variations in Holocene solar activity: Constraints from 10Be in the Greenland Ice Core Project ice core. *Journal of Geophysical Research: Space Physics 111*, A10105.

Wagner, G., Livingstone, D. M., Masarik, J., Muscheler, R. & Beer, J., 2001: Some results relevant to the discussion of a possible link between cosmic rays and the Earth's climate. *Journal of Geophysical Research: Atmospheres (1984–2012) 106*, 3381-3387.

Webber, W., Higbie, P. & Mccracken, K., 2007: Production of the cosmogenic isotopes 3H,

7Be, 10Be, and 36Cl in the Earth's atmosphere by solar and galactic cosmic rays. *Journal of Geophysical Research: Space Physics (1978–2012) 112*.

Winstrup, M., Svensson, A., Rasmussen, S. O., Winther, O., Steig, E. & Axelrod, A., 2012: An automated approach for annual layer counting in ice cores. Climate of the Past Discussions 8, 1881-1895.

Wolff, E., Bigler, M., Curran, M., Dibb, J., Frey, M., Legrand, M. & Mcconnell, J., 2012: The Carrington event not observed in most ice core nitrate records. *Geophysical research letters 39*.

Yim, M.-S. & Caron, F., 2006: Life cycle and management of carbon-14 from nuclear power generation. *Progress in Nuclear Energy 48***,** 2-36.

Zhou, D., Wang, C., Peng, Z., Rutledge, R., Sun, Y., Liang, J., Zhu, G., Zhang, S., Zhang, B. & Zhou, P., The Solar Cosmic-Ray Origin for the Rapid 14 C Increase in AD775. 2013. *33rd International Cosmic Ray Conference.*

Tidigare skrifter i serien ”Examensarbeten i Geologi vid Lunds universitet”:

361. Andolfsson, Thomas, 2013: Analyses of thermal conductivity from mineral composition and analyses by use of Thermal Conductivity Scanner: A study of thermal properties in Scanian rock types. (45 hp)
362. Engström, Simon, 2013: Vad kan inneslutningar i zirkon berätta om Varbergscharnockiten, SV Sverige. (15 hp)
363. Jönsson, Ellen, 2013: Bevarat maginnehåll hos mosasaurier. (15 hp)
364. Cederberg, Julia, 2013: U-Pb baddeleyite dating of the Pará de Minas dyke swarm in the São Francisco craton (Brazil) - three generations in a single swarm. (45 hp)
365. Björk, Andreas, 2013: Mineralogisk och malmpetrografisk studie av disseminerade sulfider i rika och fattiga prover från Kleva. (15 hp)
366. Karlsson, Michelle, 2013: En MIFO fas 1 -inventering av förorenade områden: Kvarnar med kvicksilverbetning Jönköpings län. (15 hp)
367. Michalchuk, Stephen P., 2013: The Säm fold structure: characterization of folding and metamorphism in a part of the eclogite-granulite region, Sveconorwegian orogen. (45 hp)
368. Praszkier, Aron, 2013: First evidence of Late Cretaceous decapod crustaceans from Åsen, southern Sweden. (15 hp)
369. Alexson, Johanna, 2013: Artificial groundwater recharge – is it possible in Mozambique? (15 hp)
370. Ehlorsson, Ludvig, 2013: Hydrogeologisk kartering av grundvattenmagasinet Åsumsfältet, Sjöbo. (15 hp)
371. Santsalo, Liina, 2013: The Jurassic extinction events and its relation to CO_2 levels in the atmosphere: a case study on Early Jurassic fossil leaves. (15 hp)
372. Svantesson, Fredrik, 2013: Alunskiffern i Östergötland – utbredning, mäktigheter, stratigrafi och egenskaper. (15 hp)
373. Iqbal, Faisal Javed, 2013: Paleoecology and sedimentology of the Upper Cretaceous (Campanian), marine strata at Åsen, Kristianstad Basin, Southern Sweden, Scania. (45 hp)
374. Kristinsdóttir, Bára Dröfn, 2013: U-Pb, O and Lu-Hf isotope ratios of detrital zircon from Ghana, West-African Craton – Formation of juvenile, Palaeoproterozoic crust. (45 hp)
375. Grenholm, Mikael, 2014: The Birimian event in the Baoulé Mossi domain (West African Craton) — regional and global context. (45 hp)
376. Hafnadóttir, Marín Ósk, 2014: Understanding igneous processes through zircon trace element systematics: prospects and pitfalls. (45 hp)
377. Jönsson, Cecilia A. M., 2014: Geophysical ground surveys of the Matchless Amphibolite Belt in Namibia. (45 hp)
378. Åkesson, Sofia, 2014: Skjutbanors påverkan på mark och miljö. (15 hp)
379. Härling, Jesper, 2014: Food partitioning and dietary habits of mosasaurs (Reptilia, Mosasauridae) from the Campanian (Upper Cretaceous) of the Kristianstad Basin, southern Sweden. (45 hp)
380. Kristensson, Johan, 2014: Ordovicium i Fågelsångskärnan-2, Skåne – stratigrafi och faciesvariationer. (15 hp)
381. Höglund, Ida, 2014: Hiatus - Sveriges första sällskapsspel i sedimentologi. (15 hp)
382. Malmer, Edit, 2014: Vulkanism - en fara för vår hälsa? (15 hp)
383. Stamsnijder, Joaen, 2014: Bestämning av kvartshalt i sandprov - metodutveckling med OSL-, SEM– och EDS-analys. (15 hp)
384. Helmfrid, Annelie, 2014: Konceptuell modell över spridningsvägar för glasbruksföroreningar i Rejmyre samhälle. (15 hp)
385. Adolfsson, Max, 2014: Visualizing the volcanic history of the Kaapvaal Craton using ArcGIS. (15 hp)
386. Hajny, Casandra, 2014: Ett mystiskt ryggradsdjursfossil från Åsen och dess koppling till den skånska, krittida ryggradsdjursfaunan. (15 hp)
387. Ekström, Elin, 2014: – Geologins betydelse för geotekniker i Skåne. (15 hp)
388. Thuresson, Emma, 2014: Systematisk sammanställning av större geoenergianläggningar i Sverige. (15 hp)
389. Redmo, Malin, 2014: Paleontologiska och impaktrelaterade studier av ett anomalt lerlager i Schweiz. (15 hp)
390. Artursson, Christopher, 2014: Comparison of radionuclide-based solar reconstructions and sunspot observations the last 2000 years. (15 hp)

391. Svahn, Fredrika, 2014: Traces of impact in crystalline rock – A summary of processes and products of shock metamorphism in crystalline rock with focus on planar deformation features in feldspar. (15 hp)
392. Järvin, Sara, 2014: Studie av faktorer som påverkar skredutbredningen vid Norsälven, Värmland. (15 hp)
393. Åberg, Gisela, 2014: Stratigrafin i Hanöbukten under senaste glaciationen: en studie av borrkärnor från IODP's expedition nr 347. (15 hp)
394. Westlund, Kristian, 2014: Geomorphological evidence for an ongoing transgression on northwestern Svalbard. (15 hp)
395. Rooth, Richard, 2014: Uppföljning av utlastningsgrad vid Dannemora gruva; april 2012 - april 2014. (15 hp)
396. Persson, Daniel, 2014: Miljögeologisk undersökning av deponin vid Getabjär, Sölvesborg. (15 hp)
397. Jennerheim, Jessica, 2014: Undersökning av långsiktiga effekter på mark och grundvatten vid infiltration av lakvatten – fältundersökning och utvärdering av förhållanden vid Kejsarkullens avfallsanläggning, Hultsfred. (15 hp)
398. Särman, Kim, 2014: Utvärdering av befintliga vattenskyddsområden i Sverige. (15 hp)
399. Tuvesson, Henrik, 2014: Från hav till land – en beskrivning av geologin i Skrylle. (15 hp)
400. Nilsson Brunlid, Anette, 2014: Paleoekologisk och kemisk-fysikalisk undersökning av ett avvikande sedimentlager i Barsebäcks mosse, sydvästra Skåne, bil dat för ca 13 000 år sedan. (15 hp)
401. Falkenhaug, Jorunn, 2014: Vattnets kretslopp i området vid Lilla Klåveröd: ett kunskapsprojekt med vatten i fokus. (15 hp)
402. Heingård, Miriam, 2014: Long bone and vertebral microanatomy and osteohistology of 'Platecarpus' ptychodon (Reptilia, Mosasauridae) – implications for marine adaptations. (15 hp)
403. Kall, Christoffer, 2014: Microscopic echinoderm remains from the Darriwilian (Middle Ordovician) of Västergötland, Sweden – faunal composition and applicability as environmental proxies. (15 hp)
404. Preis Bergdahl, Daniel, 2014: Geoenergi för växthusjordbruk – Möjlig anläggning av värme och kyla i Västskåne. (15 hp)
405. Jakobsson, Mikael, 2014: Geophysical characterization and petrographic analysis of cap and reservoir rocks within the Lund Sandstone in Kyrkheddinge. (15 hp)
406. Björnfors, Oliver, 2014: A comparasion of size fractions in faunal assemblages of deep-water benthic foraminifera—A case study from the coast of SW-Africa.. (15 hp)
407. Rådman, Johan, 2014: U-Pb baddeleyite geochronology and geochemistry of the White Mfolozi Dyke Swarm: unravelling the complexities of 2.70-2.66 Ga dyke swarms on the eastern Kaapvaal Craton, South Africa. (45 hp)
408. Andersson, Monica, 2014: Drumliner vid moderna glaciärer — hur vanliga är de? (15 hp)
409. Olsenius, Björn, 2014: Vinderosion, sanddrift och markanvändning på Kristianstadsslätten. (15 hp)
410. Bokhari Friberg, Yasmin, 2014: Oxygen isotopes in corals and their use as proxies for El Niño. (15 hp)
411. Fullerton, Wayne, 2014: REE mineralisation and metasomatic alteration in the Olserum metasediments. (45 hp)
412. Mekhaldi, Florian, 2014: The cosmic-ray events around AD 775 and AD 993 - Assessing their causes and possible effects on climate. (45 hp)

LUNDS UNIVERSITET

Geologiska institutionen
Lunds universitet
Sölvegatan 12, 223 62 Lund